Available online at www.sciencedirect.com
ScienceDirect
Combustion and Flame 152 (2008) 507–528
Combustion and Flame
www.elsevier.com/locate/combustflame

Remaining uncertainties in the kinetic mechanism of hydrogen combustion

Alexander A. Konnov *

Department of Mechanical Engineering, Vrije Universiteit Brussel, Brussels, Belgium

Received 12 December 2006; received in revised form 1 September 2007; accepted 30 October 2007

Available online 16 January 2008

Abstract

An analysis of the performance of an updated hydrogen combustion mechanism is presented. Particular attention was paid to different channels of reaction between H atoms and HO_2 radicals, to pressure dependence of the recombination of HO_2 radicals, and to the anomalous rate constant of reaction between OH and HO_2 radicals. The contemporary choice of the reaction rate constants is presented with the emphasis on their uncertainties. Then the predictions of ignition, oxidation, flame burning velocities, and flame structure of hydrogen–oxygen–inert mixtures are shown. The modeling range covers ignition experiments from 950 to 2700 K and from subatmospheric pressures up to 87 atm; hydrogen oxidation in a flow reactor at temperatures around 900 K from 0.3 up to 15.7 atm; flame burning velocities in hydrogen–oxygen–inert mixtures from 0.35 up to 4 atm; and hydrogen flame structure at 1 and 10 atm. Comparison of the modeling and experiments is discussed in terms of the range of applicability of the present detailed mechanism. The necessity for analysis of the mechanism to have an exhaustive list of reactions is emphasized.

Keywords: Hydrogen; Kinetic mechanism; Ignition; Oxidation; Flame

1. Introduction

Several detailed kinetic (sub-) mechanisms of hydrogen combustion have been developed recently [1–7]. These efforts were motivated by the substantial progress made in accurate measurement of the elementary reaction rates and thermodynamic properties as well as in measurement of the integral combustion characteristics such as burning velocities, ignition delays, and product formation during slow oxidation. The kinetic mechanisms of Li et al. [1] and O'Conaire et al. [2] were based on the mechanism of Mueller et al. [8]. Both these models [1,2] were validated against a wide range of experimental conditions and were found to be in good agreement with experimental data from shock tubes, flow reactors, and laminar premixed flames. Konnov [3] updated the H_2–O_2 reactions scheme of the detailed reaction mechanism for small hydrocarbon combustion [9] and also compared its performance with an extended set of experimental data from the literature. Davis et al. [5] used the H_2/CO submechanism of the GRI-mech version 3.0 [10] as a starting point and demonstrated that optimization of this model can bring very good agreement with the experiments chosen as targets. Zsély et al. [4] revised the H_2/CO reaction set of the Leeds methane oxidation mechanism [11] using the latest CEC eval-

* Fax: +32 (2) 629 28 65.
E-mail address: akonnov@vub.ac.be.

0010-2180/$ – see front matter
doi:10.1016/j.combustflame.2007.10.024

uations [12]. Particular attention has been paid in this work [4] to the uncertainties of the modeling caused by the uncertainties in the rate constants. Updates of the H_2/CO submechanism have been made by Saxena and Williams [7], and good agreement of the modeling with laminar burning velocities of hydrogen at high pressures and with extinction strain rates measured in counterflow diffusion flames was demonstrated.

Comparison of kinetic mechanisms often served to prove that one or another model is the best in predicting new experimental data. For instance, Aung et al. [13,14] compared their experimental data on H_2–O_2–N_2 flame burning velocities with the modeling employing several reaction mechanisms [15–17] and found encouraging agreement with all of them. The mechanisms of Mueller et al. [8], Marinov et al. [18], and GRI-mech version 2.11 [17] and version 3.0 [10] were tested by Kwon and Faeth [19]. They found that all the predictions reproduce experimental trends correctly, but the mechanism of Mueller et al. [8] provides the best quantitative agreement. Appel et al. [20] compared the mechanisms of Warnatz et al. [21], Mueller et al. [8], Miller and Bowman [22], and GRI-mech 3.0 [10]. They concluded that the mechanism of Warnatz et al. [21] gives the best agreement with their experimental data on catalytically stabilized combustion of hydrogen. Konnov [3] showed that at temperatures below 1000 K, the mechanism of Mueller et al. [8] overpredicts ignition delay times in stoichiometric H_2–air mixtures at 2 atm measured by Slack [23] and Snyder et al. [24] by a factor of 10, while the mechanism of Konnov [9] underpredicts them by a factor of 3–4. These experimental results in turn were correctly reproduced by the mechanism of Marinov et al. [18]. Del Alamo et al. [6] compared predictions of ignition delays of more than a dozen kinetic schemes and recommended mechanisms of Mueller et al. [8], Ranzi et al. [25], and their own as reliable at temperatures above about 1000 K and at pressures below about 50 atm. An extensive comparison of the hydrogen combustion mechanisms [8–11] has been performed by O'Conaire et al. [2], mostly to illustrate that under some experimental conditions they give very close results, while under others the difference is notable, and also to show that the changes made in the mechanism of Mueller et al. [8] have improved its performance as against these models over a wide range of conditions.

It is possible to summarize that there are several contemporary kinetic mechanisms suitable for the modeling of hydrogen combustion, among which the models of Li et al. [1] and of O'Conaire et al. [2] are probably the most extensively validated. Over the series of experiments numerically investigated with these two mechanisms the temperature ranged from 298 to 2700 K. This does not mean, however, that these models are applicable at the low temperatures encountered in the atmospheric chemistry of H_2–O_2 system. For example, effects of pressure and water dependence of the HO_2 self-reaction well established at low temperatures [26–29] were not present in the combustion mechanisms cited above. In fact, the lowest temperature accessible in experiments on hydrogen oxidation in a flow reactor was 880 K [1,2]. The chemistry of hydrogen oxidation is a core of any detailed reaction mechanism for combustion modeling, including those developed for self-ignition and oxidation of hydrocarbons at intermediate (~600 K and higher) temperatures, e.g., [25]. This means that proper extension of the hydrogen oxidation mechanism down to these temperatures requires bridging a gap between combustion and atmospheric chemistry.

It is also notable that even the list of reactions of the hydrogen combustion mechanisms is not always complete. For example, Kim et al. [15] and Mueller et al. [8] did not include the reaction

$$\mathrm{H} + \mathrm{HO_2} = \mathrm{H_2O} + \mathrm{O} \tag{13}$$

in their mechanisms, arguing that it is kinetically similar to the reaction

$$\mathrm{H} + \mathrm{HO_2} = \mathrm{OH} + \mathrm{OH}. \tag{12}$$

The models of Li et al. [1] and of O'Conaire et al. [2], both based on the mechanism of Mueller et al. [8], persevered with this omission. Although reaction (13) is not very important in slow hydrogen oxidation processes, the sensitivities of this reaction and of reaction (12) have opposite signs in laminar flames, as will be shown in the following. Thus they cannot be presumed to be kinetically similar under all conditions.

The goal of the present work was therefore to analyze the performance of the H_2–O_2 mechanism using updated kinetic and thermodynamic data and an exhaustive list of reactions. In the following, the contemporary choice of the reaction rate constants is presented with emphasis on their uncertainties. In the present work the mechanism of Konnov [3] is updated, taking into account recently evaluated kinetic data for combustion modeling [12] and for atmospheric chemistry [26]. Then predictions of ignition, oxidation, flame burning velocities, and flame structure of hydrogen–oxygen–inert mixtures are presented. Comparison of the modeling and experiments is discussed in terms of the range of applicability of the present mechanism.

2. Reaction mechanism

The detailed reaction mechanism used in this study is listed in Table 1. All reactions are reversible;

Table 1
H/O kinetic mechanism: units are cm^3 mol s cal K, $k = AT^n \exp(-E_a/RT)$, UF = uncertainty factor

No.	Reaction	A	n	E_a	Temperatures	UF	Source
1a	$H + H + M = H_2 + M$[a]	7.00E+17	−1.0	0	77–5000	2	[33][d]
	Enhanced third-body efficiencies (relative to Ar):						
	$H_2 = 0$, $N_2 = 0$, $H = 0$, $H_2O = 14.3$				300–2000	5	[33][d]
1b	$H + H + H_2 = H_2 + H_2$	1.00E+17	−0.6	0	50–5000	2.5	[33][d]
1c	$H + H + N_2 = H_2 + N_2$	5.40E+18	−1.3	0	77–2000	3.2	[33][d]
1d	$H + H + H = H_2 + H$	3.20E+15	0	0	50–5000	3.2	[33][d]
2	$O + O + M = O_2 + M$[a]	1.00E+17	−1.0	0	300–5000	2	[73][d]
	Enhanced third-body efficiencies (relative to Ar):						
	$O = 28.8$, $O_2 = 8$, $NO = 2$, $N = 2$, $N_2 = 2$,					2	[3,106][d]
	$H_2O = 5$					3	[107][e]
3	$O + H + M = OH + M$[a]	6.75E+18	−1.0	0	2950–3700	3	[36][f]
	Enhanced third-body efficiency:						
	$H_2O = 5$						[104][e]
4a	$H_2O + M = H + OH + M$[a]	6.06E+27	−3.312	120,770	300–3400	2	[35][f]
	Enhanced third-body efficiencies (relative to Ar):						[35][f]
	$H_2O = 0$, $H_2 = 3$, $N_2 = 2$, $O_2 = 1.5$						
4b	$H_2O + H_2O = H + OH + H_2O$	1.00E+26	−2.44	120,160	300–3400	2	[35][f]
5a	$H + O_2 (+M) = HO_2 (+M)$[a,b]	4.66E+12	0.44	0	300–2000	1.2	[38][d,g]
	Low-pressure limit:	5.70E+19	−1.4	0	300–2000		[38][d,g]
	$F_{cent} = 0.5$						
	Enhanced third-body efficiencies (relative to N_2):						
	$Ar = 0$, $H_2O = 0$, $O_2 = 0$, $H_2 = 1.5$, $He = 0.57$						[42][d,g,f]
5b	$H + O_2 (+Ar) = HO_2 (+Ar)$[b]	4.66E+12	0.44	0	300–2000	1.2	[38][d,g]
	Low-pressure limit:	7.43E+18	−1.2	0	300–2000		[38][d,g]
	$F_{cent} = 0.5$						
5c	$H + O_2 (+O_2) = HO_2 (+O_2)$[b]	4.66E+12	0.44	0	300–2000	1.2	[38][d,g]
	Low-pressure limit:	5.69E+18	−1.094	0	300–700	1.3	[42][d,g,f]
	$F_{cent} = 0.5$						
5d	$H + O_2 (+H_2O) = HO_2 (+H_2O)$[b]	9.06E+12	0.2	0	1050–1250	1.4	[40][d,g,f]
	Low-pressure limit:	3.67E+19	−1.0	0	1050–1250		[40][d,g,f]
	$F_{cent} = 0.8$						
6a	$OH + OH (+M) = H_2O_2 (+M)$[a,b]	1.00E+14	−0.37	0	200–1500	2.5	see text
	Low-pressure limit:	2.38E+19	−0.8	0	250–1400	2.5	[12][d]
	$F_{cent} = 0.5$						
	Enhanced third-body efficiency:						
	$H_2O = 0$						
6b	$OH + OH (+H_2O) = H_2O_2 (+H_2O)$[b]	1.00E+14	−0.37	0	200–1500	2.5	see text
	Low-pressure limit:	1.45E+18	0	0	300–400	2.5	[12,46][d]
	$F_{cent} = 0.5$						
7	$O + H_2 = OH + H$	5.06E+04	2.67	6290	297–2495	1.3	[47][d,f]
8	$H + O_2 = OH + O$	2.06E+14	−0.097	15,022	800–3500	1.5	[12][d]
9	$H_2 + OH = H_2O + H$	2.14E+08	1.52	3450	300–2500	2	[12][d]
10	$OH + OH = H_2O + O$	3.34E+04	2.42	−1930	250–2400	1.5	[12][d]
11	$HO_2 + O = OH + O_2$	1.63E+13	0	−445	220–400	1.2	[62][d]
12	$H + HO_2 = OH + OH$	1.90E+14	0	875	300–1000	2	see text
13	$H + HO_2 = H_2O + O$	1.45E+12	0	0	300	3	[12][d]
14	$H + HO_2 = H_2 + O_2$	1.05E+14	0	2047	250–1000	2	[12][d]
15	$H_2 + O_2 = OH + OH$	2.04E+12	0.44	69,155	298–1000	3	[65][g]
16	$HO_2 + OH = H_2O + O_2$[c]	2.89E+13	0	−500	250–2000	3	[12][d], see text
		+ 9.27E+15	0	17,500		3	[12][d]
17a	$HO_2 + HO_2 = H_2O_2 + O_2$[c]	1.03E+14	0	11,040	300–1250	2.5	[45][f]
		+ 1.94E+11	0	−1409		1.4	
17b	$HO_2 + HO_2 + M = H_2O_2 + O_2 + M$	6.84E+14	0	−1950	230–420	1.4	[26][d]
18	$H_2O_2 + H = HO_2 + H_2$	1.70E+12	0	3755	300–1000	3	[12][d]

(*continued on next page*)

Table 1 (*Continued*)

No.	Reaction	A	n	E_a	Temperatures	UF	Source
19	$H_2O_2 + H = H_2O + OH$	1.00E+13	0	3575	300–1000	2	[12][d]
20	$H_2O_2 + O = HO_2 + OH$	9.55E+6	2	3970	300–2500	3	[52][d]
21	$H_2O_2 + OH = HO_2 + H_2O$[c]	2.00E+12	0	427	240–1700	2	[68][f]
		+ 1.70E+18	0	29,400			

[a] All other species have efficiencies equal to unity.
[b] The fall-off behavior of this reaction is expressed in the form as used by Baulch et al. [12] and others.
[c] Rate constant is the sum of two expressions.
[d] Review.
[e] Estimate.
[f] Measurements.
[g] Theoretical calculations.

in the modeling, the reverse rate constants were calculated from the forward rate constants and thermodynamic data by the Chemkin chemical interpreter code [30]. Thermodynamic data used are all from the latest database of Burcat and Ruscic [31]. It includes recent updates of the enthalpy of formation of hydroxyl and hydroperoxyl radicals [32]. In the following, the sources of the rate constants are shortly outlined. Also, the temperature range over which the rate constants were determined and the associated uncertainty are presented. An estimated uncertainty factor, UF, implies that the rate constant is expected to be in the range $k/\mathrm{UF} < k < k \times \mathrm{UF}$. All rate coefficients in the present work are given in $\mathrm{cm}^3\,\mathrm{mol}\,\mathrm{s}$ units, while activation energies are in cal/mol.

The rate constants of hydrogen atoms' termolecular recombination with different third bodies

$$\mathrm{H} + \mathrm{H} + \mathrm{M} = \mathrm{H}_2 + \mathrm{M}, \tag{1}$$

were kept the same as in the previous mechanisms [3,9]. Baulch et al. [12] have also accepted the rates recommended by Cohen and Westberg [33] for M = H_2 and Ar with an evaluated uncertainty factor of 3 over the temperature ranges 200–5000 K and 200–2500 K, respectively. The very high collisional efficiency for H_2O estimated by Cohen and Westberg [33] was supported by Baulch et al. [12]; however, no recommendation for it was provided.

Termolecular recombination of oxygen atoms and of oxygen and hydrogen atoms,

$$\mathrm{O} + \mathrm{O} + \mathrm{M} = \mathrm{O}_2 + \mathrm{M}, \tag{2}$$

$$\mathrm{O} + \mathrm{H} + \mathrm{M} = \mathrm{OH} + \mathrm{M}, \tag{3}$$

are among the few reactions from the H_2–O_2 mechanism that were not reviewed by Baulch et al. [12].

The rate constant of oxygen atoms recombination (2) has been evaluated in a wide temperature range [52,73,111]. High-temperature measurements of the reverse reaction [112] are in very good agreement with the evaluation of Baulch et al. [111] and within 30% of Warnatz's [73] recommendation. Jerig et al. [112] determined relative collisional efficiencies as N_2:Ar = 2.1:1. Recent measurements [37,113] gave the same collisional ratio; however, the rate constants are about two times higher than those of Warnatz [73] or Jerig et al. [112]. The recommendations of Warnatz [73] are adopted here with the estimated uncertainty of a factor of 2. Krivonosova et al. [106] recommended relative collisional efficiencies $O{:}O_2{:}N{:}NO{:}N_2$ = 14.4:4:1:1:1. Accepting N_2:Ar = 2:1 [37,112], these ratios were recalculated and presented in Table 1 with an estimated uncertainty of a factor of 2.

The rate constant of reaction (3) has been determined only recently in the temperature range 2950–3700 K from the study of OH radical dissociation [36]. It was found to be in appreciable agreement with the estimate of Tsang and Hampson [52] within 300–2500 K. Naudet et al. [36] showed that the accuracy of their measurements is mostly sensitive to the value of the rate constant of reaction (1); assuming that k_1 is accurate within 30%, they derived the uncertainty of the rate constant k_3 as 30%. However, the rate constant of reaction (1) possesses an uncertainty factor of about 2 [33,46]. Taking into account this and other uncertainties, the uncertainty factor of k_3 is evaluated here as about 3.

In the previous models [3,9], the reaction of water decomposition,

$$\mathrm{H}_2\mathrm{O} + \mathrm{M} = \mathrm{H} + \mathrm{OH} + \mathrm{M}, \tag{4}$$

was written as a recombination reaction with the rate constant recommended by Baulch et al. [34], which was reconfirmed in [12]. In the present mechanism the rate constant of Srinivasan and Michael [35] was adopted. They investigated water decomposition within the range 2196–2792 K for Ar and H_2O bath gases and evaluated the accuracy of their rate expressions as ±18%. However, the scattering of reaction rates at high temperatures is still very significant. For example, recent measurements [36,37] within 2790–3200 K gave rate constants systematically lower by a factor of 4–5 than numerous literature values at

these temperatures. Taking this into account, the uncertainty is estimated as being of a factor of 2.

The temperature and pressure dependence of the rate constant of the reaction

$$H + O_2 (+M) = HO_2 (+M) \quad (5)$$

has been a subject of many recent experimental and theoretical studies. To construct a complete set of falloff curves, different high-pressure expressions were used by different authors. For example, the high-pressure rate constants of Troe [38] and of Mueller et al. [39] are very close in value, while that of Bates et al. [40] is about three times lower. For consistency, the rate constants of Troe [38] were preferred in the previous [3] and in the present mechanisms wherever possible. For water, the high-pressure and low-pressure expressions derived by Bates et al. [40] were employed. Baulch et al. [12] proposed low-pressure rate expressions that coincide for H_2O and are very close for Ar and N_2 with those cited in Table 1. The high-pressure rate expression recommended by Baulch et al. [12] cannot be directly used in the Chemkin interpreter [30]. Troe [38] proposed this expression as a sum of two terms and approximated it for the range 300–2000 K by the expression shown in Table 1. He [38] estimated a reliability of the recommended rates to be about 20%, while other experimental data [39–41] have stated accuracy to be about 30–40%. Low-pressure rate constants for Ar and N_2 as collisional partners [38–40,42] are very close, confirming the uncertainty factor evaluated by Troe [38]. Recent measurements of Hwang et al. [43] for Ar within 950–1200 K are also in close agreement with Mueller et al. [39]. The measurements of Ashman and Haynes [41] are systematically higher than that of Mueller et al. [39]; however, Scire et al. [44] concluded that they overlap, taking into account significant uncertainty in the determination of rate constants using complex reaction mechanisms. Termolecular rates at room temperature derived theoretically by Michael et al. [42] are scaled as H_2O:CH_4:O_2:H_2:Ar:He:N_2 = 12:3.5:0.74:1.51:0.49:0.57:1. These collisional efficiencies are preferred in the mechanism because they agree within 20% with the determinations of Ashman and Haynes [41] (H_2O:CO_2:Ar:N_2 = 10.6:2.4:0.56:1) and also with the earlier recommendation [34] (H_2:N_2 = 1.5:1).

One should note that the method used in the present and other models of representing different fall-off behavior of particular reactions for different collision partners by writing an individual reaction for each cannot predict appropriate high-pressure limit behavior of the mechanism. Each of the expressions reach the high-pressure limit, causing the overall reaction at the high-pressure limit to be a sum of true high-pressure limit rates. Therefore, following the approach used in, e.g., [1], only one reaction for the collision partner abundant in the mixture should be kept in the model, especially at high pressures.

At typical combustion temperatures and atmospheric pressure, the reaction

$$OH + OH (+M) = H_2O_2 (+M) \quad (6)$$

is close to its low-pressure limit. Recent measurements of the limiting low-pressure rate constant for the reverse reaction (−6) from 950 to 1250 K [45] agree well with the recommendations of Baulch et al. [46], which were adopted in the previous mechanisms [3,9] for the forward reaction. Baulch et al. [12] kept their recommendation for the low-pressure rate with H_2O; the low-pressure rate for N_2 is also very close to the earlier evaluation [46]. However, the high-pressure rate is now recommended as $1.57 \times 10^{+13}$ cm^3/(mol s) [12] only for the range 200–400 K. To extend the range of the high-pressure rate toward higher temperatures, the $T^{-0.37}$ dependence [46] was scaled up to match this value, which required about a 40% increase of the pre-exponential factor. Baulch et al. [12] improved their evaluation of the uncertainty of the rate constant over 200–400 K as being of a factor of 1.5, yet at higher temperatures it is still probably of a factor of 2.5.

Measurements by Sutherland et al. [47] of the rate constant of the reaction

$$O + H_2 = OH + H \quad (7)$$

from 504 to 2495 K were widely adopted as the most accurate so far in the review of Baulch et al. [46] and in many combustion mechanisms, e.g., [1–3,9]. Their expression [47] can be safely extrapolated up to 3500 K, since it is in good agreement with the measurements of Natarajan and Roth [48] in the overlapping range from 1713 to 3532 K, of Davidson and Hanson [49] from 2120 to 2750 K, and of Javoy et al. [50] from 2690 to 3360 K. Baulch et al. [12] proposed a different new fit to improve agreement with low-temperature measurements. This fit is very close to the high-temperature measurements mentioned above. However, it significantly deviates from the measurements and previous evaluations [46,48] at temperatures around 1000 K. Therefore, in the present model, the expression of Sutherland et al. [47] was kept.

The chain-branching reaction

$$H + O_2 = OH + O \quad (8)$$

is one of the most sensitive and important in combustion models. The rate constant recommended by Baulch et al. [46] from 300 to 5000 K was adopted in the previous mechanisms of the author [3,9]. It is notable that the rate constants k_8 used in different mechanisms can vary significantly. For example, Mueller

et al. [8] preferred the rate expression of Pirraglia et al. [51] to reproduce better their explosion limit data within 675–900 K, yet admitting that extrapolation of this rate overpredicts the recent measurements of this reaction above 1700 K. The rate constant of Pirraglia et al. [51] was kept in the model of O'Conaire et al. [2]. Some reviewers, e.g., [33,52], suggested non-Arrhenius expressions for this rate constant, which was also substantiated by the theoretical studies, e.g., [53,54]. A new expression from Baulch et al. [12] was adopted in the present mechanism. The uncertainty factors of this reaction were evaluated as 1.3 at 800 K rising to 1.5 at 3500 K [12].

A reaction converting OH radicals into H atoms,

$$H_2 + OH = H_2O + H, \tag{9}$$

attracted much attention for both theoretical and experimental reasons [55]. The rate constant recommended by Baulch et al. [46] from 300 to 2500 K was adopted in the previous mechanisms [3,9]. Baulch et al. [12] proposed a new yet very close expression based on the work of Oldenborg et al. [56] and of Krasnoperov and Michael [57]. The uncertainty factors of this reaction rate were evaluated as 1.2 at 300 K rising to 2 at 2500 K [12]. Recent very accurate measurements by Orkin et al. [58] are within 12% of the expression of Baulch et al. [12] from 250 to 479 K.

The rate constant of the reaction

$$OH + OH = H_2O + O, \tag{10}$$

suggested by Wooldridge et al. [59], has strong non-Arrhenius dependence, supported by the measurements at high [60] and at low [61] temperatures. Baulch et al. [12] proposed a new expression almost indistinguishable from the expression of Wooldridge et al. [59] and estimated uncertainty of a factor of 1.5.

The rate constant of the reaction

$$HO_2 + O = OH + O_2 \tag{11}$$

has been reliably measured only at low temperatures. Atkinson et al. [62] recommended this rate within 220–400 K. Tsang and Hampson [52] gave a very close expression up to 2500 K and estimated the uncertainty factor at these temperatures as 1.2. Baulch et al. [12] adopted the expression of Atkinson et al. [62], with uncertainty of 1.4 at 220 K rising to a factor of 3 at 1000 K. Srinivasan et al. [63] measured the reverse rate constant within 1950–2100 K and derived a forward rate that is almost 10 times higher than that from the expression adopted here [12]. This indicates a possible large uncertainty at high temperatures. Anomalous behavior (positive activation energy at high temperatures and rate constant minimum between 500 and 1500 K) cannot be excluded. Highly non-Arrhenius temperature dependence has been observed for the reactions (16), (17), and (21) discussed in the following.

The reaction between H atoms and HO_2 radicals includes three product channels,

$$H + HO_2 = OH + OH, \tag{12}$$

$$H + HO_2 = H_2O + O, \tag{13}$$

$$H + HO_2 = H_2 + O_2. \tag{14}$$

The rate constants of reactions (13) and (14) recommended by Baulch et al. [12] are adopted in this mechanism, which in turn were based on the recommendations of the IUPAC [26]. The rate constant of the formation of OH + OH (reaction (12)) was taken from Baulch et al. [46] and slightly scaled up to fit the room temperature evaluation of the IUPAC. The role of the reactions (12) and (13) and their kinetic dissimilarity will be discussed below.

The reverse reaction (−14) leads to chain initiation in hydrogen–oxygen mixtures, together with

$$H_2 + O_2 = OH + OH. \tag{15}$$

The role of initiation reactions was a subject of controversy for a long time as discussed in, e.g., [3,64]. Michael et al. [64] measured the total rate of initiation, concluded that reaction (15) is negligible, and set its rate constant to 0 in the fitting procedure. Very low values of the reaction rate k_{15} have been also confirmed by Karkach and Osherov [65]. The calculated rate constant [65] for reaction (−14) was in good agreement with the measurements and calculations of Michael et al. [64]; thus the calculated rate for reaction (15) is also assumed to be correct and it is adopted in the present mechanism. This reaction cannot compete with reaction (−14) in initiation; however, it is kept in the model for completeness, that is, to block any attempt to extend the present mechanism using outdated rate data for it.

Fig. 1 shows available measurements of the rate constant of the reaction

$$HO_2 + OH = H_2O + O_2 \tag{16}$$

at high temperatures and selected measurements at low temperatures. Many other measurements at room temperature were summarized elsewhere [12,26,62]; these data have a wide spread from 1.8×10^{13} to 7×10^{13} cm^3/mol s. Atkinson et al. [62] and Baulch et al. [12] recommended the rate constant of Keyser [66] within 250–400 K, while Baulch et al. [46] extrapolated it up to 2000 K with an uncertainty factor of 1.6 at 300 rising to 3 at 2000 K. The temperature dependence found by Keyser [66] was adopted in the mechanisms of Li et al. [1] and of O'Conaire et al. [2]. The only other determination of the temperature dependence at lower temperatures [67] is also shown in

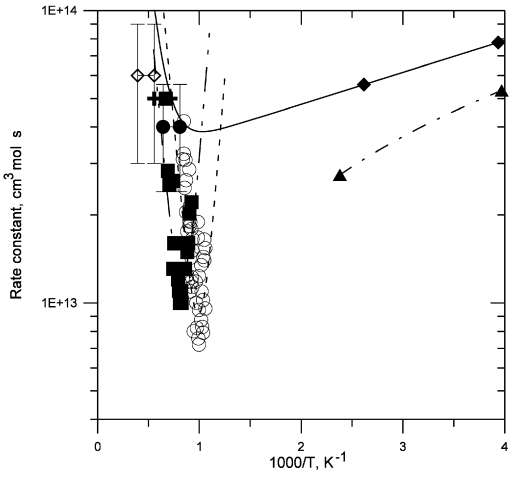

Fig. 1. Rate constant of the reaction $HO_2 + OH = H_2O + O_2$. Squares: [68], circles: [45], solid diamonds: [66], crosses: [108], open diamonds: [109], triangles: [67], solid circles: [69], solid line: present mechanism. Dashed–double dotted line and dashed line: approximation of the measurements of Hippler et al. [68] and Kappel et al. [45], respectively.

Fig. 1. Anomalous behavior (the deep and unusually narrow rate constant minimum close to 1250 K) of this reaction was observed by Hippler et al. [68] and subsequently confirmed, but at notably shifted temperature, by Kappel et al. [45]. The high-temperature part of the measurements of Hippler et al. [68] was adopted by Baulch et al. [12] as a recommendation over the range 1300–2000 K. Srinivasan et al. [69] found no evidence for the temperature dependence of the rate constant from 1237 to 1554 K. Kappel et al. [45] noted that it is difficult to combine their results with the low-temperature data. Taking into account some spread of the results of Hippler et al. [68] and Kappel et al. [45] and the latest measurements of Srinivasan et al. [69], the rate constant was approximated in the present work as a sum of two expressions from Baulch et al. [12] with an estimated uncertainty factor of 3 over the range 250–2000 K. It is clear (see Fig. 1) that the approximation adopted does not reproduce the deep and narrow rate constant minimum close to 1000 K. The effect of this assumption on the accuracy of the modeling is analyzed and discussed in the following.

The rate constant proposed by Hippler et al. [70] for the reaction

$$HO_2 + HO_2 = H_2O_2 + O_2 \tag{17a}$$

has been recommended by Baulch et al. [12,46] and adopted in many combustion mechanisms, e.g., [1,2,9], with an evaluated uncertainty factor of 1.4 between 550 and 800 K rising to 2.5 at 2500 K. Kappel et al. [45] improved the accuracy of the measurements and extended the temperature range of the new rate expression that was adopted here. Effects of pressure and water dependence of the HO_2 self-reaction well established at low temperatures [26–29] were not present in the combustion mechanisms. Baulch et al. [12] stated that at temperatures above 550 K the rate constant is pressure-independent, referring to the reviews of the IUPAC [26]. Kappel et al. [45] did not observe pressure dependence in their experiments over the range 950–1250 K, admitting, however, that some pressure dependence was detected at temperatures below 800 K. The termolecular reaction

$$HO_2 + HO_2 + M = H_2O_2 + O_2 + M \tag{17b}$$

was included in the present mechanism and its role is discussed in the following. Although the water effect on the effective rate constant is very important in atmospheric chemistry, its role vanishes at temperatures above about 400 K [26,28,29]; thus the corresponding enhancement factors have not been considered in the present model.

For two reactions between hydrogen peroxide and H atoms,

$$H_2O_2 + H = HO_2 + H_2, \tag{18}$$

$$H_2O_2 + H = H_2O + OH, \tag{19}$$

Tsang and Hampson [52] and Baulch et al. [34] proposed largely different rate constants. Lee and Hochgreb [71] suggested reducing the pre-exponential factor of the rate constant of reaction (18) by a factor of 2.1 using the activation energy of Tsang and Hampson [52] from 950 to 1050 K. The values of k_{18} derived by Lee and Hochgreb [71] are then within a factor of 2 of these of Baulch et al. [34]. For consistency, the rate expressions proposed by Baulch et al. [34] are adopted in the present mechanism for reactions (18) and (19). Baulch et al. [12] confirmed their earlier evaluation but increased the uncertainty factor for reaction (18).

The rate constant of the reaction

$$H_2O_2 + O = HO_2 + OH \tag{20}$$

was measured mostly at relatively low temperatures (see [26]) and in the only medium-temperature experiments of Albers et al. [72]. Baulch et al. [12] supported recommendations of the IUPAC within 283–500 K with the estimated uncertainty of a factor of 2. In the present work as well as in the models of Li et al. [1] and of O'Conaire et al. [2], the evaluation of Tsang and Hampson [52] was adopted. It is in good agreement with the low-temperature data [26] and with the rate of Albers et al. [72] and within a factor of 2 of the expression recommended by Warnatz [73].

The rate constant of the reaction

$$H_2O_2 + OH = HO_2 + H_2O \tag{21}$$

has been measured and analyzed in detail by Hippler et al. [68]. Subsequently its expression has been reconfirmed by Kappel et al. [45]. Baulch et al. [12] adopted this rate constant and estimated the uncertainty factor as 1.5 below 800, rising to 3 from 800 to 1700 K.

No attempt to "adjust" the reaction rate coefficients was made in the present work; however, possible modifications within the uncertainty factors listed in Table 1 will be discussed below in connection with the analysis of the mechanism performance. Particular attention was paid to the kinetic (dis)similarity of reactions (12) and (13), to the anomalous rate constant of reaction (16), and to the pressure dependence of the recombination of HO_2 radicals (17).

3. Results and discussion

3.1. Modeling details

The Senkin code from the Chemkin Collection of Codes, Release 3.6 [30], was used for the modeling of oxidation and self-ignition processes. Shock-tube and flow reactor measurements have been modeled as constant-pressure adiabatic processes. It was demonstrated, e.g., [3,74], that the calculated ignition delays in the assumption of a constant-volume process are somewhat shorter; however, the deviation is usually within a few percent, which could be neglected due to scattering of experimental data, typically within a factor of 2. Normalized sensitivity coefficients for ignition delays have been calculated using a brute force method; the computer code for this purpose was written by Kazakov [75]. The Premix code from the Chemkin Collection was used for the flame modeling. Multicomponent diffusion and thermal diffusion options were taken into account. Adaptive mesh parameters were GRAD = 0.02 and CURV = 0.5. These stringent parameters and the central differencing formulation of the convective terms were adopted to ensure accurate grid-independent solution. Transport properties from Sandia National Laboratories [30] were used. Normalized sensitivity coefficients in flow reactors and in premixed flames have been calculated using Senkin and Premix codes, respectively.

3.2. Shock tubes

Hydrogen self-ignition in mixtures with oxygen and inert gas (in most cases Ar or N_2) was extensively studied in shock tubes; relevant publications were summarized by Del Alamo et al. [6]. Shock-tube results were used to derive rate constants for the important reactions [23,76] and commonly used for kinetic model validation. The previous mechanism of

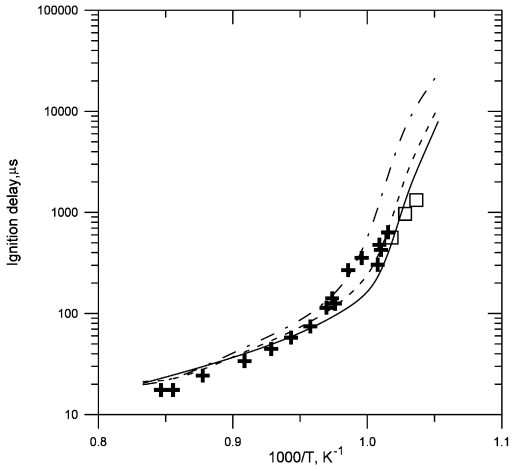

Fig. 2. Ignition delay times in stoichiometric H_2–air mixtures at 2 atm. Points: measurements; lines: calculations. Crosses: [23]; squares: [24]; solid line: the present mechanism; dashed line: the model of O'Conaire et al. [2]; dashed–dotted line: the model of Li et al. [1].

the author [3] was tested and found to be in good quantitative agreement with the ignition experiments from 950 to 2700 K and from subatmospheric pressures up to 5 atm [23,77–80]. In the present work, high-pressure measurements of Petersen et al. [81,82] and ignition delays of H_2–air–steam mixtures [74] were also used for the validation.

Fig. 2 shows ignition delay times in stoichiometric H_2–air mixtures at 2 atm [23,24]. The ignition delays, τ, were measured between the reflected shock pressure rise and the maximum positive rate of change of the OH* emission signal. Identical delays were also defined by a rapid increase in the pressure signal and by the onset of H_2O^* emission. In the modeling, however, these criteria cannot be reproduced accurately, primarily because excited species are not present in the mechanism. The ignition delay in the modeling was defined by the time when the temperature first reached a value equal to the initial one plus 200 K. One should note that employment of the default value in the Senkin code (400 K) may lead to significant disagreement with experiments, especially at higher temperatures and in significantly diluted mixtures [3]. Under the conditions of the experiments of Slack [23] and Snyder et al. [24], however, the variation of the calculated ignition delay due to this criterion (200 or 400 K) was 5% or less. Results of the calculations using the mechanism listed in Table 1 are in good quantitative agreement with the experiments. Predictions of the mechanism of O'Conaire et al. [2], also shown in Fig. 2, are very close, while the mechanism of Li et al. [1] significantly overpredicts ignition delays below 1000 K. The change of the effective ac-

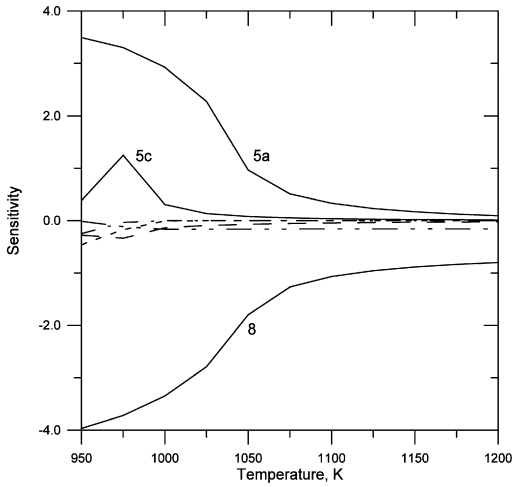

Fig. 3. Normalized sensitivities of ignition delays under the conditions of the experiments of Slack [23] and Snyder et al. [24]. Reactions H + O_2 = OH + O (8), H + O_2 (+M) = HO_2 (+M) (5a) and H + O_2 (+O_2) = HO_2 (+O_2) (5c) are marked on the graph. Short dashed line: H_2O_2 + H = HO_2 + H_2 (18); long dashed line: H + HO_2 = 2OH (12); dashed–dotted line: 2OH (+M) = H_2O_2 (+M) (6a); dashed–double-dotted line: O + H_2 = OH + H (7).

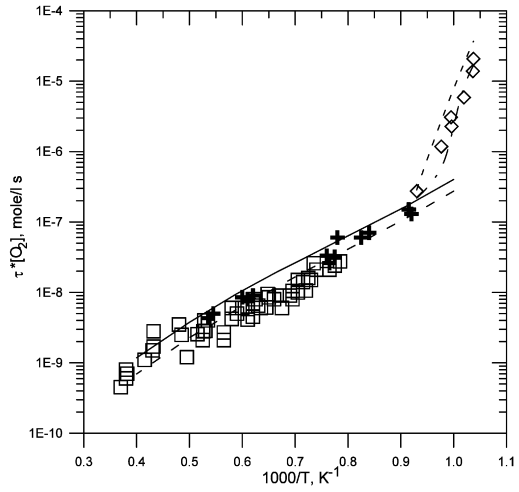

Fig. 4. Ignition delay times in H_2–O_2–Ar mixtures. Points: experiments; lines: present calculation. Diamonds and dashed–dotted line: 8% H_2–2% O_2, $P = 5$ atm [77]; crosses and solid line: 1% H_2–2% O_2, $P = 1$ atm; squares and dashed line: 4% H_2–2% O_2, $P = 1$ atm [78]. Short-dashed line: calculations with the models [1,2] for 8% H_2–2% O_2, $P = 5$ atm.

tivation energy at temperatures below about 1025 K is accurately reproduced by these three models. At these temperatures, the experimental conditions approach the second explosion limit, and the calculated ignition delays are extremely sensitive to the rate constant of reaction (5) [18,23]. Sensitivity analyses of Slack [23] and Marinov et al. [18] also revealed that reaction (8) is important at all temperatures, while other reactions exhibited very low sensitivities. Slack [23] performed a sensitivity analysis at 1000 K for two mixture compositions, while Marinov et al. [18] analyzed sensitivities at 1000 and 1111 K. Fig. 3 shows normalized sensitivities of ignition delays throughout the range of temperatures calculated with the present mechanism, which are in qualitative agreement with the previous studies [18,23]. The sensitivity analysis has been performed in this work not only to endorse general understanding of the combustion chemistry of hydrogen, but mainly to search for the conditions where "controversial" reactions could be manifested. It was found that the reactions

$$H + HO_2 = OH + OH, \tag{12}$$

$$H + HO_2 = H_2O + O \tag{13}$$

both have negative signs of the sensitivity coefficients, while the absolute value of the sensitivity for reaction (13) is much lower, and thus it cannot be discriminated from reaction (12) through comparison of the modeling with the ignition delays. The reaction

$$HO_2 + OH = H_2O + O_2 \tag{16}$$

has negligibly small sensitivity, and therefore the deep and narrow rate constant minimum close to 1000 K (Fig. 1) does not affect overall model predictions of the ignition delays. The pressure-dependent reaction

$$HO_2 + HO_2 + M = H_2O_2 + O_2 + M \tag{17b}$$

has a sensitivity about an order of magnitude smaller than that of the reaction

$$HO_2 + HO_2 = H_2O_2 + O_2 \tag{17a}$$

under the conditions of the experiments of Slack [23] and Snyder et al. [24].

Prior to the correlation formula for ignition delays in H_2–O_2–Ar mixtures derived by Cheng and Oppenheim [80], many authors presented their data by plotting the temperature dependence of the product of τ and initial oxygen concentration, e.g., [76,78,84]. To compare their results with the earlier measurements of Schott and Kinsey [78], Skinner and Ringrose [77] plotted these data on the same graph, as shown in Fig. 4. The ignition delays below 1200 K correspond to the maximum in the OH* emission [77]; they were defined in the modeling as the time until the maximum of the ground state OH concentration. The ignition delays above 1200 K correspond to the threshold of detectability of OH concentrations, approximately 10^{-6} mol/l [78]. The same criterion has been used in the calculations also presented in Fig. 4. The ignition delays in a wide temperature range, as well as the change in the effective activation energy observed under higher pressures and temperatures below 1000 K

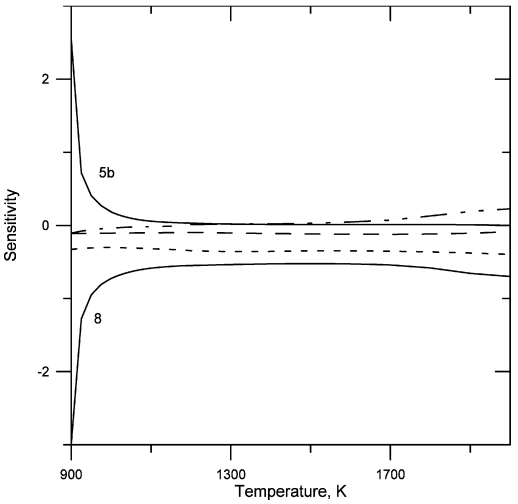

Fig. 5. Normalized sensitivities of ignition delays under the conditions of the experiments with 1% H_2–2% O_2, $P = 1$ atm [78]. Reactions $H + O_2 = OH + O$ (8), $H + O_2$ (+Ar) = HO_2 (+M) (5b) are marked on the graph. Short dashed line: $O + H_2 = OH + H$ (7), long dashed line: $H_2 + OH = H_2O + H$ (9), dashed–dotted line: $H + HO_2 = 2OH$ (12), dashed–double-dotted line: $OH + OH = H_2O + O$ (10).

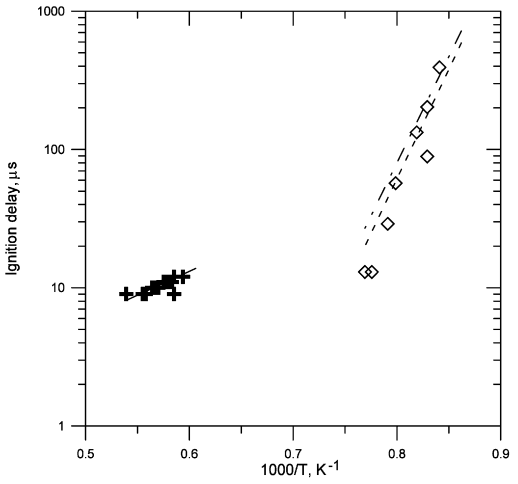

Fig. 6. Ignition delay times in stoichiometric H_2–O_2–Ar mixtures. Points: experiment, $P = 33$ atm [81,82]; lines: present calculations. Crosses and solid line: 0.5% H_2–0.25% O_2; diamonds and dashed line: 2% H_2–1% O_2. Dashed–dotted line: calculations with the models [1,2] for 2% H_2–1% O_2.

[77], are correctly reproduced by the modeling with the present mechanism and with the models of Li et al. [1] and of O'Conaire et al. [2]. At temperatures above 1200 K, predictions of the models [1,2] (not shown in Fig. 4) are also very close to the measurements; at lower temperatures they are almost indistinguishable from each other and are shown in Fig. 4 as a single curve. The differences between the performance of the present model and the models [1,2] will be analyzed in the following.

A sensitivity analysis of the ignition in rich 8% H_2–2% O_2–Ar mixture performed by Maas and Warnatz [85] showed that the calculated ignition delays are mostly affected by the rate constant of the chain-branching reaction (8) from low (900 K) to high (1500 K) temperatures. Reaction (5) is a chain-terminating process, while reaction (14) serves as an initiation process at high and as a terminating one at intermediate (1100 K) temperatures. Fig. 5 shows normalized sensitivities of ignition delays throughout the range of temperatures calculated with the present mechanism for the lean mixture 1% H_2–2% O_2 at 1 atm under the conditions of the experiments of Schott and Kinsey [78]. Briefly summarizing the results of the sensitivity analysis presented in Figs. 3 and 5, together with those from the literature, one can conclude that at temperatures below about 1100 K hydrogen ignition delays are mostly sensitive to reactions (8) and (5), and, in fact, they are controlled by the ratio of these rate constants with minor impact of other reactions. At higher temperatures the role of reaction (5) rapidly vanishes, while other reactions could be important, depending on the mixture stoichiometry.

Petersen et al. [81,82] measured ignition delay times in stoichiometric H_2–O_2–Ar mixtures based on $(d[OH]/dt)_{max}$ from laser absorption of OH at 306 nm. The same criterion has been used in the present calculations. Although the stoichiometry of the mixtures was fixed, a wide range of concentrations (0.1–2% for H_2), temperatures (1189–1930 K), and pressures (33–87 atm) made these results a valuable benchmark for validation of kinetic models. Experimental data together with calculated ignition delays are shown in Figs. 6–8. The present mechanism and the models of Li et al. [1] of O'Conaire et al. [2] accurately reproduce ignition delays throughout the range of pressures and temperatures. A small difference between predictions of the models [1,2] and of the present one is found only at temperatures below 1300 K (Fig. 6), yet it is within the scattering of the measurements.

Overall good agreement with the experiments enables analysis of the model behavior at high pressures. Normalized sensitivities of ignition delays from 1000 to 1250 K were calculated with the present mechanism for the stoichiometric mixture 2% H_2–1% O_2–Ar at 33 atm (see Fig. 6). Similarly to the sensitivity analysis shown in Figs. 3 and 5, reactions (8) and (5) were found to be the most sensitive. Due to much higher pressure as compared to the conditions of Figs. 3 and 5, the role of the recombination reactions

$$HO_2 + HO_2 = H_2O_2 + O_2, \qquad (17a)$$

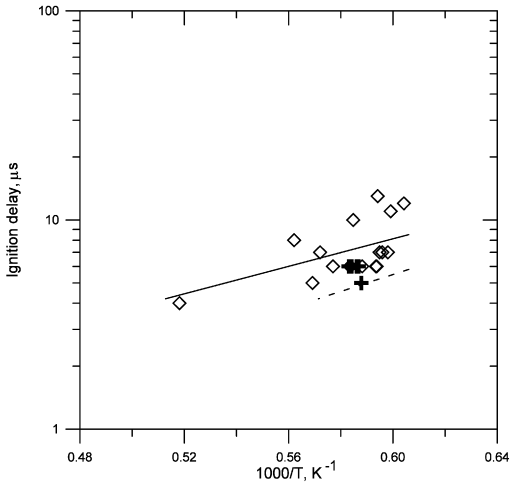

Fig. 7. Ignition delay times in stoichiometric 0.5% H_2–0.25% O_2–Ar mixture. Points: experiment [81,82]; lines: present calculations. Diamonds and solid line: 57 atm; crosses and dashed line: 87 atm.

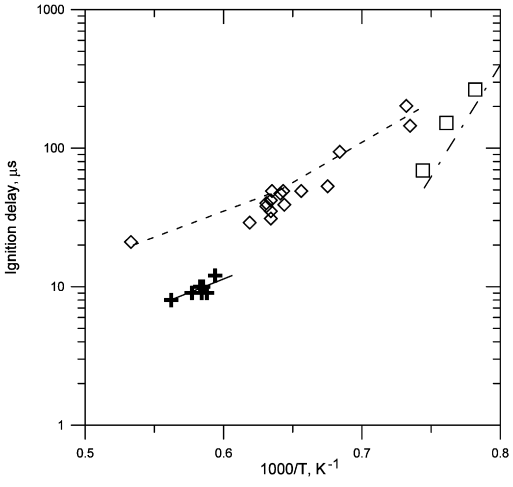

Fig. 8. Ignition delay times in stoichiometric H_2–O_2–Ar mixtures. Points: experiment, $P = 64$ atm [81,82]; lines: present calculations. Crosses and solid line: 0.33% H_2–0.167% O_2; diamonds and dashed line: 0.1% H_2–0.05% O_2; squares and dashed–dotted line: 0.5% H_2–0.25% O_2.

$$HO_2 + HO_2 + M = H_2O_2 + O_2 + M \qquad (17b)$$

is not negligible. In the mixture 2% H_2–1% O_2–Ar at 33 atm, normalized sensitivities of these two reactions are about −0.2 at 1000 K and almost linearly approach 0 with temperature increase up to 1250 K. Removal of reaction (17b) from the model increases calculated ignition delay at 1000 K by 28% at 33 atm and by 44% at 87 atm. This reaction is even more important in lean mixtures and lower temperatures. Somewhat longer ignition delays predicted by the models [1,2] as compared to the present mechanism (Fig. 6) could be partially due to the missing reaction (17b).

In relation to this analysis it is interesting to compare the experimental results on hydrogen autoignition at high pressures and intermediate temperatures around 1000 K and the modeling performed by Mittal et al. [86]. Ignition delays of H_2–O_2–N_2–Ar mixtures were measured in a rapid compression machine and compared with predictions of several models [1,2,5,10]. At 30 atm the best agreement was found with the mechanism of O'Conaire et al. [2], while other models overpredicted ignition delays. At 15 atm the calculated results show a slope of the Arrhenius plot steeper than the slope of the measured values. Finally, at 50 atm, all cited models overpredicted ignition delays and disagreement increased toward lower temperatures. In the present work, the ignition delays obtained in a rapid compression machine [86] have not been modeled because this requires experimental pressure profiles. It is clear, however, that inclusion of the pressure-dependent reaction (17b) could potentially improve performance of the models at lower temperatures and higher pressures.

Additional examples of model validation are presented in Appendix A. The quality of the agreement of the present mechanism and other mechanisms, e.g., [1,2], with the hydrogen ignition experiments in shock tubes at high temperatures from subatmospheric pressures up to 87 atm is about the same. However, predictive capabilities of these models toward lower temperatures (Fig. 2) and higher pressures (Fig. 6) are not. Ignition delays in the mixture 1% H_2–1% O_2–Ar were calculated at 900 K using these three models. With the pressure increase from 1 to 87 atm the present mechanism predicts an increase of the ignition delay by a factor of 28; the mechanism of Li et al. [1] by a factor of 22; and the mechanism of O'Conaire et al. [2] by a factor of 14. Clearly, new experimental data are required to validate these models at temperatures intermediate between typical combustion and slow oxidation.

3.3. Hydrogen oxidation in a flow reactor

Hydrogen oxidation in a flow reactor was studied by Yetter et al. [87] and by Mueller et al. [8]. These measurements were extensively used for the validation of hydrogen mechanisms [1,2], implicitly assuming plug flow adiabatic conditions. However, modeling of the experiments in the flow reactor has some peculiarities related to the finite mixing time, effects of mass diffusion, and wall surface reactions. The effects of mass diffusion and wall surface reactions were found to be important in the evaluation of chemical reaction rates from laminar flow reactor

data [88]. Significant uncertainty in the determination of rate constants from the flow reactor data using complex reaction mechanisms has been revealed by Scire et al. [44].

The common problem of flow reactors is the inability to convert experimental profiles as a function of axial distance into time profiles [87]. This problem is usually overcome by shifting the experimental data to match the calculated data at a reference point of 50% consumption of the major reactant. In the present work this assumption was validated numerically. It was found that inhomogeneous mixing of the reactants affects only the initial part of the calculated concentration profiles; the major portion of the profiles and their slopes after complete mixing remain unchanged even if the imperfect mixing is accompanied by artificial injection of initiating radicals. Zsély et al. [4] considered time shifting as an independent uncertainty and, after analysis of the modeling under the conditions of the measurements performed by Yetter et al. [87], concluded that "Very different parameter sets can describe this experiment appropriately." This statement is incorrectly formulated, as was illustrated by O'Conaire et al. [2] through comparison of several different mechanisms with the same experimental data. Uncertainty analysis should be performed not for the time shift (ignition delay in a flow reactor) and species concentrations, but for the slopes of the species profiles. In fact, large uncertainties of the modeling revealed for the hydrogen oxidation in a flow reactor [4] signify high sensitivity of the mechanism predictions to uncertainties in rate constants. The same conclusion is applicable to ignition delays at lower temperatures and to laminar burning velocities of hydrogen in rich flames. In other words, ignition delays at lower temperatures, laminar burning velocities of hydrogen in rich flames, and measurements in a flow reactor at intermediate temperatures are the most valuable data for hydrogen mechanism validation; other experimental data can indeed be modeled by different parameter sets.

Flow reactors are not completely adiabatic, and heat losses may significantly complicate modeling, especially under conditions close to explosive limits [15]. A combined effect of the mass diffusion, radical losses on the reactor walls, and heat losses can manifest itself through flattening of the apparent spatial profiles of temperature and species concentration as compared to the calculated ones. For example, the experimental species profiles and temperature in the mixture 0.5% H_2–0.5% O_2–N_2 at 0.3 atm and initial temperature of 880 K [8] are compared with the adiabatic calculations using the present reaction mechanism in Fig. 9. Small (about 5 K) but notable deviations of the calculated temperature profile from the measured one cause slightly steeper predicted concentration profiles. Similar deviation of the calculated adiabatic temperature profile from the measurements has been observed in the original work [8]. In the present work the measurements shown in Fig. 9 were also modeled with the experimental temperature profile. The difference between adiabatic and nonadiabatic calculations does not exceed the stated accuracy of the species concentration measurements (±5% [8]).

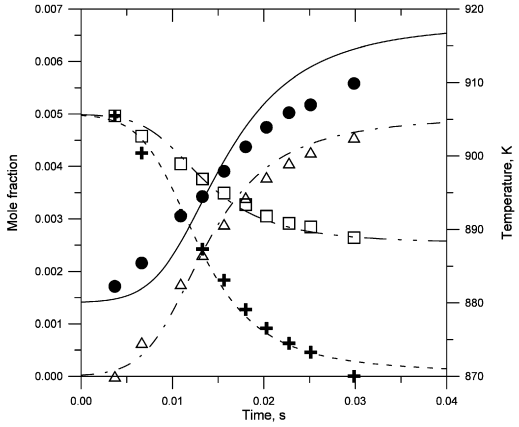

Fig. 9. Species profiles and temperature in the mixture 0.5% H_2–0.5% O_2–N_2 at 0.3 atm and $T_{in} = 880$ K. Points: measurements [8]; lines: adiabatic calculations. Circles and solid line: temperature; crosses and dashed line: H_2; triangles and dashed–dotted line: H_2O; squares and dashed–double-dotted line: O_2.

At higher pressures, the temperature profiles were not reported [8]; therefore a comparison cannot be conclusive under conditions close to explosive limits [15]. Hydrogen profiles in the lean ($\phi \sim 0.3$) mixtures H_2–O_2–N_2 at 6.5 atm and varying initial temperature [8] are shown in Fig. 10. The modeling using the present mechanism is also shown and found to be in good agreement with the experiments. This set of experiments involves double scanning through the temperature: by initial temperature of the mixture from 884 to 934 K and in each run due to heating up of the mixture. It was therefore interesting to analyze the possible influence of the deep and narrow rate constant minimum of the reaction

$$HO_2 + OH = H_2O + O_2 \tag{16}$$

on the calculated profiles of hydrogen consumption. To do so, the rate constant measured by Hippler et al. [68] was approximated by the expression

$$k = 9.27 \times 10^{+15} \exp(-17{,}500/RT) + 1.3 \times 10^{+9} \exp(20{,}000/RT),$$

shown by the dashed–double-dotted line in Fig. 1; the rate constant measured by Kappel et al. [45] was ap-

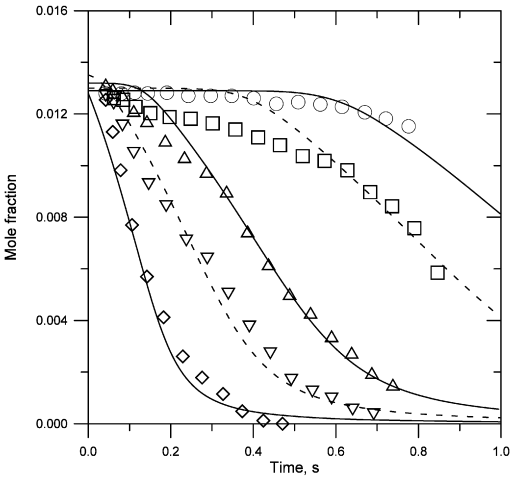

Fig. 10. Hydrogen profiles in the lean mixtures H_2–O_2–N_2 at 6.5 atm and varying initial temperature. Points: measurements [8]; lines: adiabatic calculations. Circles: 1.29% H_2–2.19% O_2 at 884 K; squares: 1.3% H_2–2.21% O_2 at 889 K; triangles: 1.32% H_2–2.19% O_2 at 906 K; upside triangles: 1.36% H_2–2.24% O_2 at 914 K; diamonds: 1.36% H_2–2.24% O_2 at 934 K.

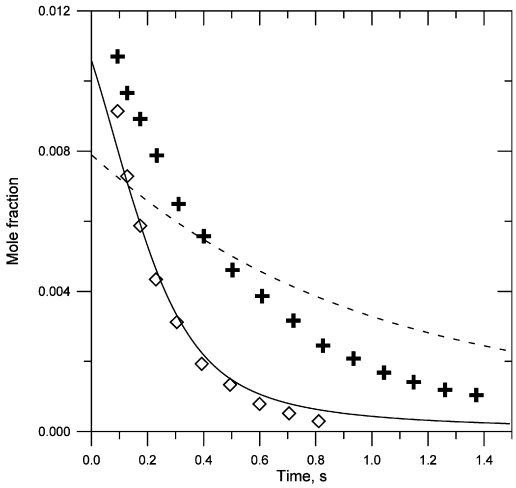

Fig. 11. Hydrogen concentration in the stoichiometric and lean mixtures at 15.7 atm and $T_{in} = 914$ K. Points: measurements [8]; lines: adiabatic calculations. Crosses and dashed line: 1.18% H_2–0.61% O_2–N_2; diamonds and solid line: 1.18% H_2–2.21% O_2–N_2.

proximated by the expression

$$k = 3 \times 10^{+16} \exp(-17{,}500/RT) + 2 \times 10^{+8} \exp(20{,}000/RT)$$

shown by the dashed line in Fig. 1. The first expression has its minimum close to 1250 K and can be used down to about 950 K, while the second one has its minimum close to 1000 K and can be used down to 820 K. The use of the first expression in the model gave results very close to the predictions of the base mechanism listed in Table 1, because all experiments were performed at temperatures below 943 K [8]. One can conclude that available flow reactor data cannot confirm or reject the existence of the rate constant minimum found by Hippler et al. [68]. It is also notable that Srinivasan et al. [69] found no evidence for temperature dependence of the rate constant from 1237 to 1554 K; at temperatures below 1250 K the measurements of Kappel et al. [45] are close in absolute values of the rates but possess the opposite temperature dependence.

Employment of the second expression dramatically accelerates the rate of hydrogen consumption. Close to the reference point of 50% consumption of hydrogen, the rate increases 2.5 times at 934 K and 2.1 times at 889 K, which corresponds to additional effective activation energy of ~6.4 kcal/mol due to rapid increase of the rate constant of reaction (16) toward lower temperatures. Mueller et al. [8] found effective overall activation energy of 61 ± 10 kcal/mol, which was compared to 58.3 kcal/mol from the steady-state analysis and to 57 kcal/mole from other experiments. Since the value of additional effective activation energy (6.4 kcal/mol) is within the experimental uncertainty, no conclusion could be made on the applicability of the rate constant measured by Kappel et al. [45]; more accurate experiments and/or extended data processing are required to clarify this issue.

The experimental hydrogen concentrations in the lean mixture at 15.7 atm and initial temperature of 914 K [8] are reproduced very well by the adiabatic calculations (Fig. 11). Yet, in the stoichiometric mixture, the difference between the modeling and the measurements is far beyond the experimental uncertainties. Reactions (12), (13), and (16) and the pressure dependence of the recombination of HO_2 radicals (17) were first screened to reveal the reason for the discrepancy. Reaction (13) does not noticeably affect the modeling in a flow reactor. Employment of the rate expression for reaction (16), which mimics the results of Kappel et al. [45], accelerates hydrogen oxidation under both lean and stoichiometric conditions by approximately the same factor. Normalized sensitivities of the recombination reactions (17a) and (17b) are almost identical at 15.7 atm; they are also very close in the lean and in the stoichiometric mixtures. One can conclude that the reactions in question similarly affect the rate of hydrogen oxidation under the conditions of the experiments shown in Fig. 11 and therefore cannot be responsible for deterioration of the present mechanism performance in the stoichiometric mixture at 15.7 atm.

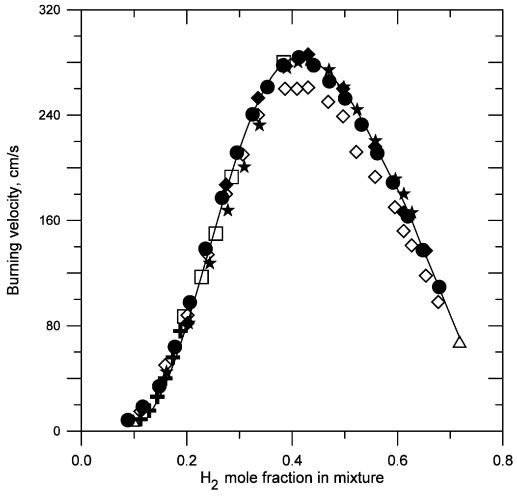

Fig. 12. Measured (points) and calculated (line) unstretched laminar burning velocities for hydrogen–air flames at standard temperature and pressure. Crosses: [90]; squares: [89]; open diamonds: [13,14]; solid diamonds: [19]; circles: [91]; triangles: [92]; stars: [93].

In contrast to the present mechanism, the models of Li et al. [1] and of O'Conaire et al. [2] accurately reproduce all available experiments in the flow reactor. A sensitivity analysis of hydrogen consumption in the two mixtures shown in Fig. 11 has been performed and compared with the analyses performed for ignition delays (Figs. 3 and 5). The only good candidate for improving the performance of the present model in the stoichiometric mixture at 15.7 atm, while keeping satisfactory agreement with the ignition experiments discussed above and with laminar flame burning velocities presented below, was found to be the reaction

$$H + HO_2 = H_2 + O_2. \quad (14)$$

At 914 K the rate constant of this reaction employed in [1,2] is almost three times lower than that used in the present mechanism. Lower values of this rate constant significantly accelerate the rate of hydrogen consumption in a flow reactor in a stoichiometric mixture much less affecting it in lean mixture. However, decrease of this rate constant makes the calculated ignition delays significantly shorter at the low-temperature end of the experiments shown in Figs. 2 and 4, since reaction (14) serves as an initiation process at high and as a terminating one at intermediate (1100 K) and lower temperatures.

3.4. Hydrogen flame burning velocities

Fig. 12 shows measured and calculated laminar burning velocities of hydrogen–air flames at standard initial temperature (298 K) and atmospheric pressure as a function of the hydrogen mole fraction in the mixture. Most of the recent measurements are generally consistent within experimental uncertainties, while those of Aung et al. [13,14] are notably lower than others in rich flames. Burning velocities of hydrogen–air mixtures as a function of temperature, pressure, and stoichiometric ratio have been measured by many investigators; however, the data were incompatible for a long time. Wu and Law [89] were apparently the first who demonstrated experimentally that the flame stretch due to flame front curvature and/or flow divergence must be taken into account in the data processing. The methodology of the determination of laminar burning velocities with the counterflow twin-flame technique by extrapolation to zero stretch rate has been further improved by Vagelopoulos et al. [90]. In constant-volume bombs, the unstretched burning velocities of hydrogen–air mixtures were determined in several groups [13,14,19,91–95] using essentially the same approach. The experimental uncertainty of the laminar burning velocities derived from expanding spherical flames was estimated [13,19] to be about 10%. The uncertainty of the counterflow twin-flame technique is limited by the accuracy of the LDV, which was estimated to be 1–2 cm/s for burning velocities less than 60 cm/s and up to 10 cm/s for those above 170 cm/s [96]. The calculations are in good agreement with the experimental data obtained by extrapolation to zero stretch rates for the whole range of equivalence ratios (Fig. 12).

Unstretched laminar burning velocities of hydrogen flames at high pressures are available for a limited number of combinations of the mixture contents and pressure, mostly from constant volume bombs [14,19, 93,96,97]. Additional experimental uncertainty of this method is related to the conventional conversion of the displacement flame speed into the flame burning velocity using the stretch-independent density ratio of the unburned mixture and burned gases. This approach may introduce an added discrepancy (less than 10%) primarily at lower pressures and large hydrogen concentrations near limits [19]. The systematic measurements in hydrogen–air mixtures [14] are shown in Fig. 13 and compared with the model predictions. It is remarkable that the calculated burning velocities rapidly converge with the experiments as the pressure increases. Good agreement of these experiments with the calculations could not be expected in rich mixtures at atmospheric and moderate pressures because the measurements of Aung et al. [13,14] were found to be consistently lower than other data from the literature (see Fig. 12).

Measurements of laminar burning velocities were also conducted using a new technique based on particle tracking velocimetry and image processing for

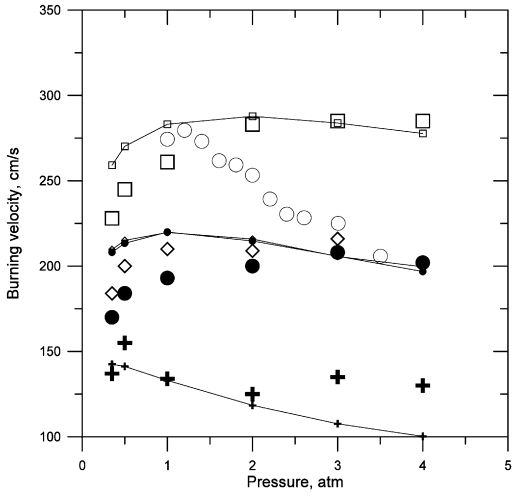

Fig. 13. Unstretched laminar burning velocities for hydrogen–air flames at standard temperature as a function of initial pressure. Measurements: symbols; calculations: lines with corresponding small symbols. Equivalence ratios: crosses: 0.75; diamonds: 1.05; squares: 1.8 [14]; solid circles: 3 [14]; open circles: 3 [98].

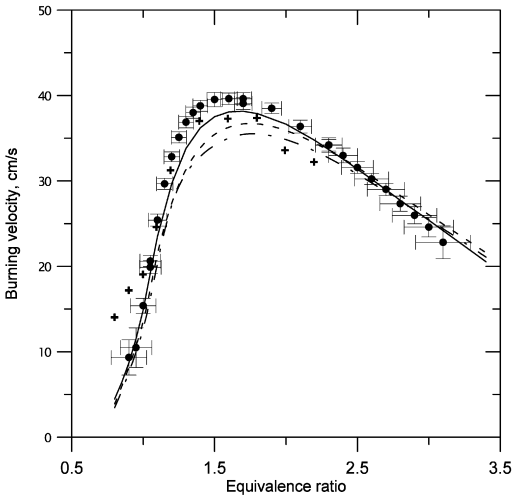

Fig. 14. Unstretched laminar burning velocities for H_2–O_2–N_2 flames at standard temperature and pressure. Dilution ratio $O_2/(O_2 + N_2) = 0.077$. Points: measurements; lines: modeling. Crosses: counterflow twin-flame technique [96]; circles: heat flux method [100]. Solid line: modeling with the present mechanism; dashed line: the mechanism of Li et al. [1]; dashed–dotted line: the mechanism of O'Conaire et al. [2].

burner-stabilized flames in a high-pressure chamber [98]. These results for equivalence ratio 3 are shown in Fig. 13 to illustrate significant disagreement of the available experimental data at elevated pressures, which is much higher than the expected experimental uncertainty.

Sensitivity analyses of the hydrogen–air flames have been performed in many studies; the most instructive one was presented by Brown et al. [99]. The authors demonstrated that the individual uncertainties of the H/O reactions cited by Baulch et al. [34,46] and combined with the reaction sensitivities lead to an overall estimated uncertainty in the computed burning velocities of about 8–10% from lean to moderately rich flames. Thus one can conclude that reexamination of the key H/O reactions via comparison of experimental burning velocities with model predictions is not justified when the discrepancy is well within the experimental uncertainty. New accurate measurements of hydrogen burning velocities are therefore extremely important for model validation.

Hermanns et al. [100] determined laminar adiabatic burning velocities of flames propagating in hydrogen–oxygen–nitrogen mixtures at atmospheric pressure. Fig. 14 shows selected results of this study obtained in the mixtures with dilution ratio $O_2/(O_2 + N_2) = 0.077$. Experimental error margins were defined for a 95% confidence interval. Also shown are the measurements performed by the counterflow twin-flame technique [96]. These experiments are compared in Fig. 14 with the predictions of the present mechanism, the mechanism of Li et al. [1], and the mechanism of O'Conaire et al. [2]. All three models are in very good agreement with the burning velocities in lean and in rich mixtures; however, it is only the present mechanism that satisfactorily predicts burning velocities in the fastest flames. Additional examples of the model validation are presented in Appendix A.

Uncertainty analysis of the simulation results in the present work was performed at the conditions of the experiments of Hermanns et al. [100] at equivalence ratios 0.8, 1, 2, and 3. The following procedure was employed: each rate constant was separately replaced by the values k/UF and $k \times \mathrm{UF}$, where UF is the uncertainty factors listed in Table 1. Uncertainty factors of collisional efficiencies were not taken into account in the present analysis. Modification of the rate constant of reaction (i) results either in the increase of the burning velocity, Δ_i^+, or in its decrease, Δ_i^-. Although this brute force method of uncertainty analysis is time-consuming, it is believed that it is more accurate than approach based on local sensitivities [99], because in most cases these variations were not symmetric, that is, $\Delta_i^+ \neq -\Delta_i^-$. The uncertainty of the calculated burning velocity was defined as $(\Delta_{\mathrm{Su}}^{3\sigma})^2 = \sum_i ((\Delta_i^+)^2 + (\Delta_i^-)^2)/2$ on the assumption that the extreme values k/UF and $k \times \mathrm{UF}$ correspond to the rate constants' distribution within a 3σ interval. The following 1σ uncertainties of the calculated burning velocities were thus obtained: 19.9% at equivalence ratio $\phi = 0.8$, 16.2% at $\phi = 1$, 12.9%

at $\phi = 2$, and 16.6% at $\phi = 3$. These uncertainties are qualitatively different from those calculated for hydrogen–air flames [4,99]. In lean and stoichiometric hydrogen–air flames the uncertainties of the modeling were relatively small, rapidly increasing toward rich flames, while in the highly diluted H_2–O_2–N_2 flames [100], great sensitivity of the mechanism predictions to uncertainties in rate constants is observed throughout the range of equivalence ratios.

Uncertainty analysis described above also presents a direct measure of the influence of different reactions on the calculated burning velocity. The reaction

$$H + HO_2 = OH + OH \quad (12)$$

was found among a few with high sensitivity in laminar flames [1,2,99]. However, the reaction

$$H + HO_2 = H_2O + O \quad (13)$$

did not appear in the sensitivity spectra of the earlier studies because it was not included in the models [1,2,8,15]. The present analysis showed that indeed the absolute value of the sensitivity of the burning velocity to the rate constant of reaction (13) is about 10 times smaller than that of reaction (12) at all equivalence ratios, yet the sensitivities of this reaction and of reaction (12) have opposite signs. Thus these reactions cannot be presumed to be kinetically similar at all conditions.

3.5. Hydrogen flame structure

Hydrogen flame structure studies at atmospheric and higher pressures are very scarce [101–103]. A fuel-rich atmospheric-pressure flame at an initial temperature of 336 K [102] has been thoroughly analyzed by Dixon-Lewis [104] and is frequently used as a benchmark for the validation of kinetic models. The concentration profiles of hydrogen, oxygen, and water normalized by nitrogen concentration in an 18.83% H_2–4.6% O_2–76.57% N_2 flame are shown in Fig. 15. Experimental temperature profile and reported linear burning velocity [102] were used as input data for the modeling. The present calculations accurately reproduce the concentration profiles and spatial gradients of the major species.

A similar technique of flame probe sampling was used to study stoichiometric flames of 10% H_2–5% O_2–85% Ar mixture at 1 and 10 atm and initial temperature 363 K [103]. The spatial resolution of the probe was about 0.1 mm. At 1 atm, the flame front thickness was ~2 mm and good agreement between the measured profiles and the modeling was found (not shown here). At 10 atm, the experimentally observed flame front thickness decreases to 0.7 mm (Fig. 16). The calculations using experimental temperature profile and reported flow rate are also shown

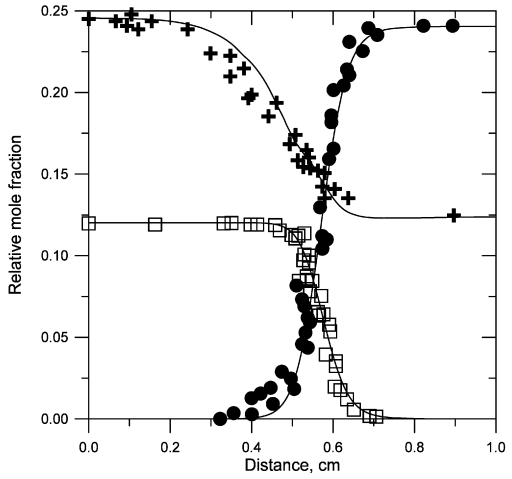

Fig. 15. Concentration profiles of hydrogen, oxygen, and water normalized by nitrogen concentration in 18.83% H_2–4.6% O_2–76.57% N_2 flame at atmospheric pressure and initial temperature of 336 K. Points: experiment [102]; crosses: H_2; squares: $O_2 \times 2$; circles: $H_2O \times 2$; lines: present calculations.

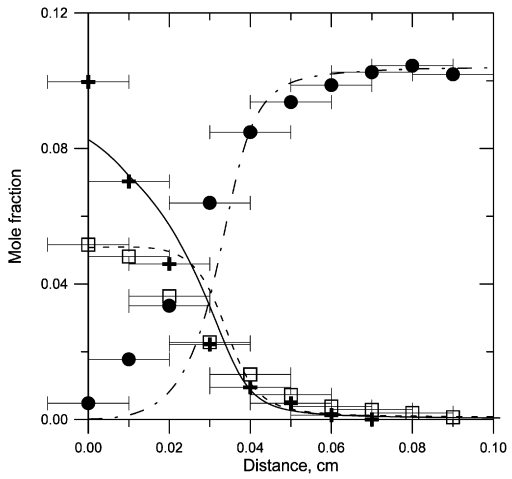

Fig. 16. Concentration profiles of hydrogen, oxygen, and water in 10% H_2–5% O_2–85% Ar flame at 10 atm and initial temperature 363 K. Points: experiment [103]; lines: present calculations; crosses and solid line: H_2; squares and dashed line: O_2; circles and dashed–dotted line: H_2O.

in Fig. 16. The agreement is satisfactory, yet the calculated profiles are somewhat steeper than the experimental ones. There are two apparent reasons for this discrepancy. First, the concentrations measured by the probe having spatial resolution of about 0.1 mm [103] are spatially averaged values; thus, the steep gradients cannot be accurately resolved. Spatial error bars shown in Fig. 16 illustrate the size of the probing volume. Second, in the modeling of high-

pressure flames, the common assumption of an ideal gas is not very accurate, as demonstrated by El-Gamal et al. [105]. The authors found that at 10 atm real gas modeling predicts somewhat lower hydrogen–air flame burning velocities and a slightly higher flame front thickness as compared to the ideal gas calculations shown in Fig. 16. The remaining uncertainties in the rate constants of the pressure-dependent reactions can also contribute to the deficiencies of the modeling at elevated pressures. Normalized sensitivities for HO_2 concentrations with respect to the recombination reactions

$$HO_2 + HO_2 = H_2O_2 + O_2, \quad (17a)$$

$$HO_2 + HO_2 + M = H_2O_2 + O_2 + M \quad (17b)$$

have been calculated in the high-pressure flame shown in Fig. 16. The negative sensitivities of both reactions peak near the burner surface in the cold zone; the maximum values of these sensitivities are very close at 10 atm. Further downstream these sensitivities rapidly approach zero and could be considered unimportant after about 0.03 cm from the burner (cf. Fig. 16).

4. Concluding remarks

In spite of apparent simplicity, contemporary reaction mechanisms for the H_2–O_2 system developed by different authors often differ by the number of reactions and their rate constants. The goal of the present work was to analyze the performance of the H_2–O_2 mechanism using updated kinetic and thermodynamic data and an exhaustive list of reactions. It was demonstrated that the reactions

$$H + HO_2 = OH + OH, \quad (12)$$

$$H + HO_2 = H_2O + O \quad (13)$$

have the same sign of the sensitivity coefficients in the modeling of ignition delays and slow oxidation of hydrogen in a flow reactor; the absolute value of the sensitivity for reaction (13) is much lower, and thus it cannot be discriminated from reaction (12) through comparison of the modeling with such experiments. However, the sensitivities of the burning velocity to the rate constants of reaction (13) and of reaction (12) have opposite signs. Thus these reactions are kinetically different and should both be considered in contemporary reaction schemes.

It is a common practice to use hydrogen combustion mechanisms validated at temperatures above ~800 K in the models developed for self-ignition and oxidation of hydrocarbons at intermediate (~600 K) temperatures. It was demonstrated in the present work that pressure dependence of the recombination of HO_2 radicals due to the reaction

$$HO_2 + HO_2 + M = H_2O_2 + O_2 + M \quad (17b)$$

could be of importance even at temperatures around 1000 K at high pressures, especially in lean mixtures. When included, this reaction potentially extends the range of the mechanism validity down to ~400 K. Neither the present mechanism nor the literature models cited above include the recombination reaction

$$O + OH + M = HO_2 + M.$$

It could be important under the conditions when recombination of O atoms (reaction (2)) and/or of OH radicals (reaction (6)) are important. Further analysis of the impact of this reaction should be performed, which is the objective of the author.

The second group of remaining uncertainties in the kinetic mechanism of hydrogen combustion are associated with the rate constants employed. These uncertainties were discussed and summarized in Table 1. They can be directly used in the analysis of the uncertainties of the modeling caused by the uncertainties in the rate constants. Particular attention was paid to the anomalous rate constant of the reaction

$$HO_2 + OH = H_2O + O_2. \quad (16)$$

It was impossible to confirm or reject the existence of the deep and narrow rate constant minimum close to 1250 K found by Hippler et al. [68] through comparison of the modeling with available experimental data, mostly due to insensitivity of the ignition delays to this reaction. The rate constant of reaction (16) measured by Kappel et al. [45] has its minimum close to 1000 K and could manifest itself through significant acceleration of the predicted hydrogen oxidation rate in a flow reactor. Acceptance of their values would require significant modifications of the rate constants of other key reactions, which will have an adverse effect on the overall model performance. More accurate experiments in a flow reactor and/or extended data processing are required to clarify this issue.

Results of the calculations performed in this work using the updated mechanism are in good quantitative agreement with the ignition experiments from 950 to 2700 K and from subatmospheric pressures up to 87 atm. The kinetic scheme has also been compared with the experimental data on hydrogen oxidation in the flow reactor at temperatures around 900 K. General good agreement was found between the measurements at 0.3, 1, and 6.5 atm and the simulation results. At higher pressure (15.7 atm), the experimental hydrogen concentrations are reproduced quite well in the lean mixture. The rate of hydrogen oxidation in the stoichiometric mixture was significantly underpredicted. Since no attempt to "adjust" the reaction rate coefficients was made in the

present work, this discrepancy indicates remaining uncertainty in the present mechanism and calls for further analysis. The experimental measurements of the flame burning velocities in hydrogen–oxygen–inert mixtures show large disparities at high pressures. The modeling results agree well with the recent measurements throughout the range of equivalence ratios when flame stretch and curvature effects have been taken into account in the data processing. Scarce measurements of the hydrogen flame structure are also reproduced well at atmospheric pressure. At 10 atm, the agreement is satisfactory; however, the calculated profiles are steeper than the experimental ones.

Acknowledgments

Financial support of this work by the European Government within the "Safekinex" Project EVG1-CT-2002-00072 is gratefully acknowledged.

Appendix A. Additional examples of the model validation

A.1. Shock tubes

Cheng and Oppenheim [80] determined ignition delays in stoichiometric and lean H_2–O_2–Ar mixtures from pressure records at pressures from 1.7 to 2.5 atm within the temperature range 1000–1430 K. They presented these results as a single plot normalized by the hydrogen and oxygen concentrations (Fig. A.1). In the modeling, the density of the mixtures after the shock wave was assumed to be 2.13×10^{-2} mol/l. Fig. A.1 shows the calculations at constant pressure with critical heating-up of 200 K for the mixture 6.7% H_2–3.3% O_2–Ar. The ignition delays [80] were defined as the time elapsed from the moment when the reaction was initiated to the instant when the energy release attained 1% of maximum [83]. In the modeling, this corresponds to the heating-up of the mixture by much less than 200 K, yet the calculated ignition delays are only slightly shorter than that shown in Fig. A.1, as discussed elsewhere [3].

Asaba et al. [79] measured ignition delays in H_2–O_2–Ar mixtures of different composition at pressures from 0.2 to 0.5 atm within the temperature range 1400–2500 K. The ignition delays correspond to the threshold of detectability of OH concentrations, which was assumed to be 10^{-8} mol/l. Further analysis of these data [76] showed that variation of this threshold value from 10^{-7} to 10^{-6} mol/l increases calculated ignition delays by about 40% especially at the higher temperatures of this study. In the present calculations the threshold value of 2.5×10^{-7} mol/l

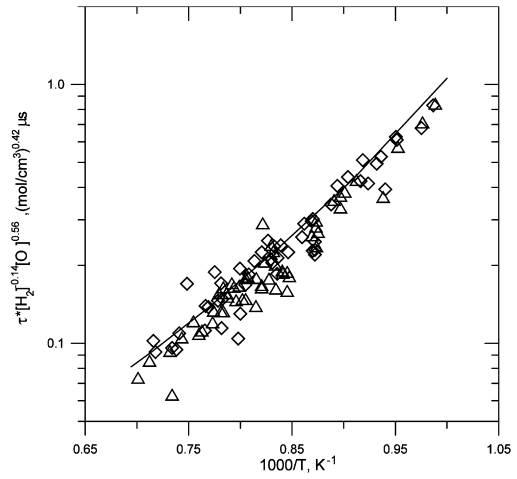

Fig. A.1. Normalized ignition delay times in H_2–O_2–Ar mixtures, $P = 1.75$–2.5 atm. Triangles: 6.7% H_2–3.3% O_2; diamonds: 5% H_2–5% O_2 [80]. Solid line: calculations at constant pressure with critical heating-up of 200 K.

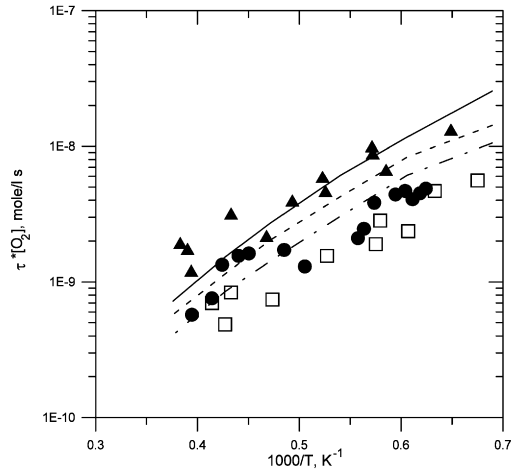

Fig. A.2. Ignition delay times in H_2–O_2–Ar mixtures. Points: experiment, $P = 0.22$–0.4 atm [79]; lines: present calculations. Triangles and solid line: 1% H_2–3% O_2; circles and dashed line: 1% H_2–1% O_2; squares and dashed–dotted line: 3% H_2–1% O_2.

[76] was chosen. The density of the mixtures after the shock wave was assumed to be 1.85×10^{-3} mol/l; thus the calculated pressures vary from 0.22 to 0.4 atm. The ignition delays normalized by the initial oxygen concentration are shown in Fig. A.2 and compared with the modeling. The agreement can be considered as satisfactory, taking into account uncertainties of the experiments and simplified assumptions in the calculations.

Ignition delay times in H_2–air–steam mixtures were measured by Wang et al. [74] and compared

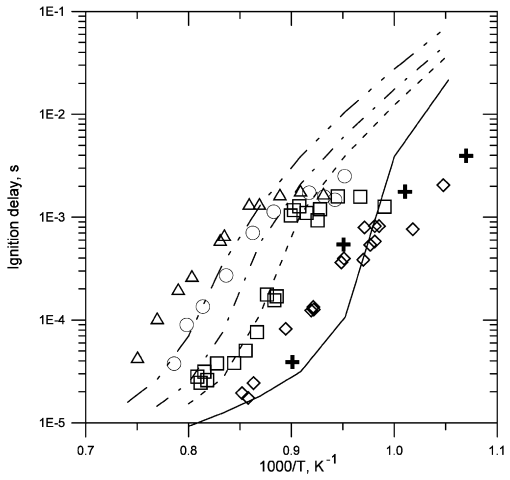

Fig. A.3. Ignition delay times in H_2–air–steam mixtures. Points: experiment, $P = 3$–5 atm [74]; lines: present calculation at 4 atm. Diamonds [74], crosses [110], and solid line: 15% H_2–85% air; squares and dashed line: 12.75% H_2–72.25% air–15% steam; circles and dashed–dotted line: 11.25% H_2–63.75% air–25% steam; triangles and dashed–double-dotted line: 9% H_2–51% air–40% steam.

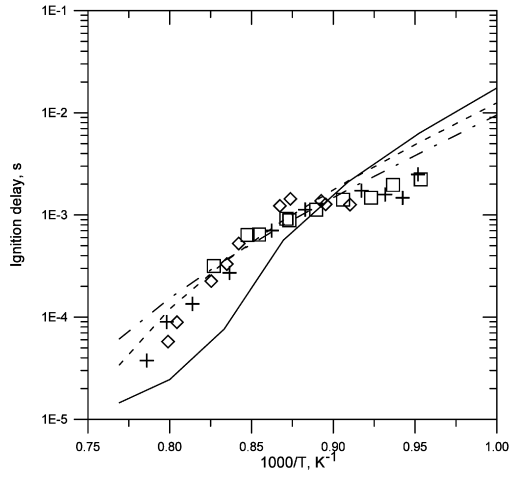

Fig. A.4. Influence of pressure on ignition delay times in 11.25% H_2–63.75% air–25% steam mixture. Points: experiment [74]. Crosses: 4–5 atm; diamonds: 9–10 atm; squares: 15–17 atm. Lines: present calculation. Solid line: 4 atm; dashed line: 9.5 atm; dashed–dotted line: 16 atm.

with several kinetic models including GRI-mech, version 2.11 [17] and version 3.0 [10], Konnov [9], and Miller and Bowman [22], and with the mechanism compiled from the evaluation of Baulch et al. [46]. All these models predicted quite different results at temperatures around 1000 K even in a dry H_2–air mixture. O'Conaire et al. [2] reported good agreement of their mechanism with ignition delays in the mixture containing 25% steam, while in 0% and 15% steam mixtures the measured ignition delays were a lot shorter than those predicted by the model below 1010 and 1090 K, respectively. Experimental results at pressures 3–5 atm [74] are shown in Fig. A.3, and the influence of pressure on ignition delay times in 11.25% H_2–63.75% air–25% steam mixture is shown in Fig. A.4. The ignition delays were measured between the reflected shock pressure rise and the maximum positive rate of change of the OH* emission signal. Identical delays were also defined by a rapid increase in the pressure signal. In the modeling they were defined as the time until the maximum of the ground state OH concentration. The present calculations quantitatively reproduce the small pressure dependence at higher pressures of the study; also, the temperature shift of the ignition delays toward higher temperatures caused by increased amounts of steam is in satisfactory agreement with the measurements. However, the range of validity of the present mechanism as compared to the experiments in H_2–air–steam mixtures [74] should be, probably, assigned not to the range of temperatures or pressures, but to the range

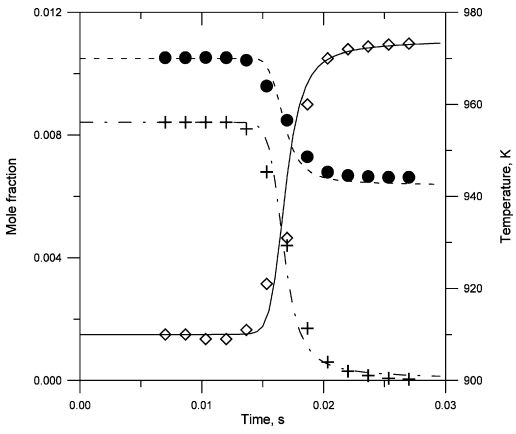

Fig. A.5. Species profiles and temperature in the mixture 0.842% H_2–1.052% O_2–N_2 at 1 atm and $T_{in} = 910$ K. Points: measurements [87]; lines: adiabatic calculations. Diamonds and solid line: temperature; crosses and dashed–dotted line: H_2; circles and dashed line: O_2.

of ignition delay times shorter than 1 ms. It is notable that throughout the temperature range 900–1350 K no ignition delay longer than 3 ms was observed. It is quite possible that for some experimental reasons, after 1 ms, mixture uniformity was broken down, which caused forced ignition manifested in unexpectedly short ignition delays.

A.2. Flow reactor

Species and temperature profiles in the mixture 0.842% H_2–1.052% O_2–N_2 at 1 atm and initial temperature of 910 K are shown in Fig. A.5. Due to a

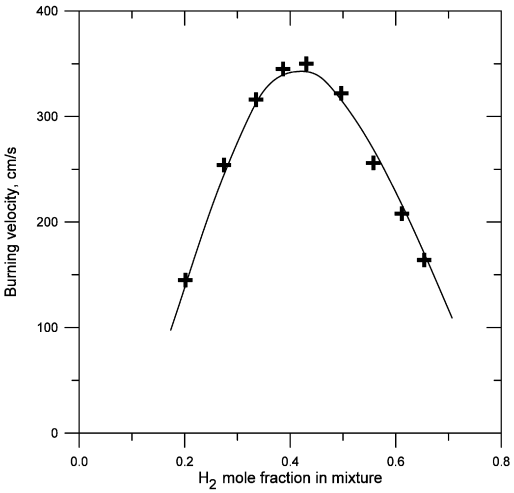

Fig. A.6. Measured [19] and calculated (line) unstretched laminar burning velocities for hydrogen–oxygen–argon flames at standard temperature and pressure. $O_2/(O_2 + Ar) = 0.21$.

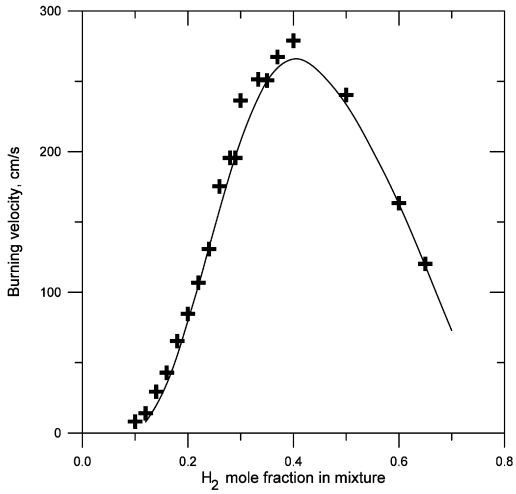

Fig. A.7. Measured [94] and calculated (line) unstretched laminar burning velocities for hydrogen–oxygen–nitrogen flames at initial temperature 295 K and pressure 750 Torr. $O_2/(O_2 + N_2) = 0.2$.

misprint in the original manuscript [87], this graph was often attributed to the mixture 0.842% H_2–1.52% O_2–N_2, and, surprisingly, good agreement was found. Sensitivity analysis confirmed that initial oxygen concentration in this lean mixture has little effect on the calculated profiles of H_2 and temperature. Present adiabatic plug flow calculations also shown in Fig. A.5 accurately reproduce experimental data.

A.3. Laminar burning velocities

Fig. A.6 shows measured [19] and calculated unstretched laminar burning velocities for hydrogen–oxygen–argon flames ($O_2/(O_2 + Ar) = 0.21$) at standard temperature and pressure. Replacement of the diluent affects thermal properties of the mixtures as well as importance of the third-body reactions of recombination and decomposition. Overall effect is accurately captured by the model.

Some unresolved inconsistency and scattering of the experimental data can be explained by the loosely defined temperature, pressure and composition of the initial mixtures studied. Fig. A.7 demonstrates that when these initial conditions are well defined, the agreement of the measurements and the modeling is very good. Small reduction of the initial temperature (295 K instead of 298 K), pressure (750 Torr), and oxygen content in the artificial air ($O_2/(O_2 + N_2) = 0.2$) [94] yield burning velocities essentially very close to the experimental data assigned to the standard conditions (Fig. A.7).

Supplementary material

The online version of this article contains additional supplementary information.

Please visit DOI: 10.1016/j.combustflame.2007.10.024.

References

[1] J. Li, Z. Zhao, A. Kazakov, F.L. Dryer, Int. J. Chem. Kinet. 36 (2004) 566–575.
[2] M. O'Conaire, H.J. Curran, J.M. Simmie, W.J. Pitz, C.K. Westbrook, Int. J. Chem. Kinet. 36 (2004) 603–622.
[3] A.A. Konnov, Khim. Fiz. 23 (8) (2004) 5–18.
[4] I.Gy. Zsély, J. Zádor, T. Turányi, Proc. Combust. Inst. 30 (2005) 1273–1281.
[5] A.G. Davis, A.V. Joshi, H. Wang, F. Egolfopoulos, Proc. Combust. Inst. 30 (2005) 1283–1292.
[6] G. Del Alamo, F.A. Williams, A.L. Sanchez, Combust. Sci. Technol. 176 (2004) 1599–1626.
[7] P. Saxena, F.A. Williams, Combust. Flame 145 (2006) 316–323.
[8] M.A. Mueller, T.J. Kim, R.A. Yetter, F.L. Dryer, Int. J. Chem. Kinet. 31 (1999) 113–125.
[9] A.A. Konnov, Detailed reaction mechanism for small hydrocarbons combustion, Release 0.5, 2000; http://homepages.vub.ac.be/~akonnov/.
[10] G.P. Smith, D.M. Golden, M. Frenklach, N.W. Moriarty, B. Eiteneer, M. Goldenberg, C.T. Bowman, R.K. Hanson, S. Song, W.C. Gardiner Jr., V.V. Lissianski, Z. Qin, GRI-Mech 3.0, 1999; http://www.me.berkeley.edu/gri_mech/.
[11] K.J. Hughes, T. Turanyi, A.R. Clague, M.J. Pilling, Int. J. Chem. Kinet. 33 (2001) 513–538.

[12] D.L. Baulch, C.T. Bowman, C.J. Cobos, R.A. Cox, T. Just, J.A. Kerr, M.J. Pilling, D. Stocker, J. Troe, W. Tsang, R.W. Walker, J. Warnatz, J. Phys. Chem. Ref. Data 34 (3) (2005) 757–1397.
[13] K.T. Aung, M.I. Hassan, G.M. Faeth, Combust. Flame 109 (1997) 1–24.
[14] K.T. Aung, M.I. Hassan, G.M. Faeth, Combust. Flame 112 (1998) 1–15.
[15] T.J. Kim, R.A. Yetter, F.L. Dryer, Proc. Combust. Inst. 25 (1994) 759–766.
[16] W. Wang, B. Rogg, Combust. Flame 94 (1993) 271–292.
[17] M. Frenklach, H. Wang, C.T. Bowman, R.K. Hanson, G.P. Smith, D.M. Golden, W.C. Gardiner Jr., V.V. Lissianski, GRI-Mech 2.11, 1995; http://www.me.berkeley.edu/gri_mech/.
[18] N. Marinov, C.K. Westbrook, W.J. Pitz, in: S.H. Chan (Ed.), Transport Phenomena in Combustion, vol. 1, Taylor and Francis, Washington, DC, 1996.
[19] O.C. Kwon, G.M. Faeth, Combust. Flame 124 (2001) 590–610.
[20] C. Appel, J. Mantzaras, R. Schaeren, R. Bombach, A. Inauen, B. Kaeppeli, B. Hemmerling, A. Stampanoni, Combust. Flame 128 (2002) 340–368.
[21] J. Warnatz, R.W. Dibble, U. Maas, Combustion, Physical and Chemical Fundamentals, Modeling and Simulation, Springer-Verlag, New York, 1996.
[22] J.A. Miller, C.T. Bowman, Prog. Energy Combust. Sci. 15 (1989) 287–338.
[23] M.W. Slack, Combust. Flame 28 (1977) 241–249.
[24] A.D. Snyder, J. Robertson, D.L. Zanders, G.B. Skinner, Technical Report AFAPL-TR-65-93, 1965; citation from Slack [23].
[25] E. Ranzi, P. Gaffuri, T. Faravelli, P. Dagaut, Combust. Flame 103 (1995) 91–106.
[26] R. Atkinson, D.L. Baulch, R.A. Cox, J.N. Crowley, R.F. Hampson, R.G. Hynes, M.E. Jenkin, M.J. Rossi, J. Troe, Atmos. Chem. Phys. 4 (2004) 1461–1738.
[27] C.C. Kircher, S.P. Sander, J. Phys. Chem. 88 (10) (1984) 2082–2091.
[28] N. Kanno, K. Tonokura, A. Tezaki, M. Koshi, J. Phys. Chem. A 109 (14) (2005) 3153–3158.
[29] D. Stone, D.M. Rowley, Phys. Chem. Chem. Phys. 7 (10) (2005) 2156–2163.
[30] R.J. Kee, F.M. Rupley, J.A. Miller, M.E. Coltrin, J.F. Grcar, E. Meeks, H.K. Moffat, A.E. Lutz, G. Dixon-Lewis, M.D. Smooke, J. Warnatz, G.H. Evans, R.S. Larson, R.E. Mitchell, L.R. Petzold, W.C. Reynolds, M. Caracotsios, W.E. Stewart, P. Glarborg, C. Wang, O. Adigun, Chemkin Collection, Release 3.6, Reaction Design, Inc., San Diego, CA, 2000.
[31] A. Burcat, B. Ruscic, Third Millennium Ideal Gas and Condensed Phase Thermochemical Database for Combustion with updates from Active Thermochemical Tables, ANL-05/20 and TAE 960 Technion–IIT, Aerospace Engineering, and Argonne National Laboratory, Chemistry Division, September 2005; ftp://ftp.technion.ac.il/pub/supported/aetdd/thermodynamics; accessed January 2006.
[32] B. Ruscic, R.E. Pinzon, M.L. Morton, N.K. Srinivasan, M.-C. Su, J.W. Sutherland, J.V. Michael, J. Phys. Chem. A 110 (2006) 6592–6601.
[33] N. Cohen, K.R. Westberg, J. Phys. Chem. Ref. Data 12 (1983) 531.
[34] D.L. Baulch, C.J. Cobos, R.A. Cox, C. Esser, P. Frank, Th. Just, J.A. Kerr, M.J. Pilling, J. Troe, R.W. Walker, J. Warnatz, J. Phys. Chem. Ref. Data 21 (1992) 411.
[35] N.K. Srinivasan, J.V. Michael, Int. J. Chem. Kinet. 38 (2006) 211–219.
[36] V. Naudet, S. Javoy, C.E. Paillard, Combust. Sci. Technol. 164 (2001) 113–128.
[37] S. Javoy, V. Naudet, S. Abid, C.E. Paillard, Exp. Therm. Fluid Sci. 27 (2003) 371–377.
[38] J. Troe, Proc. Combust. Inst. 28 (2000) 1463–1469.
[39] M.A. Mueller, R.A. Yetter, F.L. Dryer, Proc. Combust. Inst. 27 (1998) 177–184.
[40] R.W. Bates, D.M. Golden, R.K. Hanson, C.T. Bowman, Phys. Chem. Chem. Phys. 3 (2001) 2337–2342.
[41] P.J. Ashman, B.S. Haynes, Proc. Combust. Inst. 27 (1998) 185–191.
[42] J.V. Michael, M.-C. Su, J.W. Sutherland, J.J. Carroll, A.F. Wagner, J. Phys. Chem. A 106 (2002) 5297–5313.
[43] S.M. Hwang, S.-O. Ryu, K.J. De Witt, M.J. Rabinowitz, Chem. Phys. Lett. 408 (2005) 107–111.
[44] J.J. Scire, F.L. Dryer, R.A. Yetter, Int. J. Chem. Kinet. 33 (2001) 784–802.
[45] Ch. Kappel, K. Luther, J. Troe, Phys. Chem. Chem. Phys. 4 (2002) 4392–4398.
[46] D.L. Baulch, C.J. Cobos, R.A. Cox, P. Frank, G. Hayman, Th. Just, J.A. Kerr, T. Murrells, M.J. Pilling, J. Troe, R.W. Walker, J. Warnatz, Combust. Flame 98 (1994) 59–79.
[47] J.W. Sutherland, J.V. Michael, A.N. Pirraglia, F.L. Nesbitt, R.B. Klemm, Proc. Combust. Inst. 21 (1988) 929–941.
[48] K. Natarajan, P. Roth, Combust. Flame 70 (1987) 267–279.
[49] D.F. Davidson, R.K. Hanson, Combust. Flame 82 (1990) 445–447.
[50] S. Javoy, V. Naudet, S. Abid, C.E. Paillard, Int. J. Chem. Kinet. 32 (2000) 686–695.
[51] A.N. Pirraglia, J.V. Michael, J.W. Sutherland, R.B. Klemm, J. Phys. Chem. 93 (1989) 282–291.
[52] W. Tsang, R.F. Hampson, J. Phys. Chem. Ref. Data 15 (1986) 1087–1279.
[53] J.A. Miller, B.C. Garrett, Int. J. Chem. Kinet. 29 (1997) 275–287.
[54] H. Teitelbaum, A. Lifshitz, Phys. Chem. Chem. Phys. 2 (2000) 687–692.
[55] I.W.M. Smith, F.F. Crim, Phys. Chem. Chem. Phys. 4 (2002) 3543–3551.
[56] R.C. Oldenborg, G.W. Loge, D.M. Harradine, K.R. Winn, J. Phys. Chem. 96 (1992) 8426–8430.
[57] L.N. Krasnoperov, J.V. Michael, J. Phys. Chem. A 108 (2004) 5643–5648.
[58] V.L. Orkin, S.N. Kozlov, G.A. Poskrebyshev, M.J. Kurylo, J. Phys. Chem. A 110 (2006) 6978–6985.
[59] M.S. Wooldridge, R.K. Hanson, C.T. Bowman, Int. J. Chem. Kinet. 26 (1994) 389–401.
[60] J.W. Sutherland, P.M. Patterson, R.B. Klemm, Proc. Combust. Inst. 23 (1991) 51–57.
[61] Y. Bedjanian, G. Le Bras, G. Poulet, J. Phys. Chem. A 103 (1999) 7017–7025.

[62] R. Atkinson, D.L. Baulch, R.A. Cox, R.F. Hampson Jr., J.A. Kerr, M.J. Rossi, J. Troe, J. Phys. Chem. Ref. Data 26 (1997) 1329–1499.
[63] N.K. Srinivasan, M.C. Su, J.W. Sutherland, J.V. Michael, J. Phys. Chem. A 109 (2005) 7902–7914.
[64] J.V. Michael, J.W. Sutherland, L.B. Harding, A.F. Wagner, Proc. Combust. Inst. 28 (2000) 1471–1478.
[65] S.P. Karkach, V.I. Osherov, J. Chem. Phys. 110 (1999) 11918–11927.
[66] L.F. Keyser, J. Phys. Chem. 92 (1988) 1193–1200.
[67] U.C. Sridharan, L.X. Qiu, F. Kaufman, J. Phys. Chem. 88 (1984) 1281–1282.
[68] H. Hippler, H. Neunaber, J. Troe, J. Chem. Phys. 103 (1995) 3510–3516.
[69] N.K. Srinivasan, M.C. Su, J.W. Sutherland, J.V. Michael, B. Ruscic, J. Phys. Chem. A 110 (2006) 6602–6607.
[70] H. Hippler, J. Troe, J. Willner, J. Chem. Phys. 93 (1990) 1755–1760.
[71] D. Lee, S. Hochgreb, Int. J. Chem. Kinet. 30 (1998) 385–406.
[72] E.A. Albers, K. Hoyermann, H.G. Wagner, J. Wolfrum, Proc. Combust. Inst. 13 (1971) 81.
[73] J. Warnatz, in: W.C. Gardiner Jr. (Ed.), Combustion Chemistry, Springer-Verlag, New York, 1984, p. 197.
[74] B.L. Wang, H. Olivier, H. Gronig, Combust. Flame 133 (2003) 93–106.
[75] A. Kazakov, personal communication, 2004.
[76] D.L. Ripley, W.C. Gardiner Jr., J. Chem. Phys. 44 (1966) 2285–2296.
[77] G.B. Skinner, G.H. Ringrose, J. Chem. Phys. 42 (1965) 2190–2192.
[78] G.L. Schott, J.L. Kinsey, J. Chem. Phys. 29 (1958) 1177–1182.
[79] T. Asaba, W.C. Gardiner Jr., R.F. Stubbeman, Proc. Combust. Inst. 10 (1965) 295–302.
[80] R.K. Cheng, A.K. Oppenheim, Combust. Flame 58 (1984) 125–139.
[81] E.L. Petersen, D.F. Davidson, M. Rohrig, R.K. Hanson, in: 31st AIAA/ASME/SAE/ASEE Joint Propulsion Conference and Exhibit, San Diego, 1995, AIAA 95-3113.
[82] E.L. Petersen, D.F. Davidson, M. Rohrig, R.K. Hanson, in: Proceedings of the 20th International Symposium on Shock Waves, Pasadena, 1995, pp. 941–946.
[83] A.K. Oppenheim, L.M. Cohen, J.M. Short, R.K. Cheng, K. Hom, Proc. Combust. Inst. 15 (1974) 1503–1513.
[84] L.J. Drummond, Aust. J. Chem. 20 (1967) 2331–2341.
[85] U. Maas, J. Warnatz, Combust. Flame 74 (1988) 53–69.
[86] G. Mittal, C.-J. Sung, R.A. Yetter, Int. J. Chem. Kinet. 38 (2006) 516–529.
[87] R.A. Yetter, F.L. Dryer, H. Rabitz, Combust. Sci. Technol. 79 (1991) 129–140.
[88] J.C. Lee, R.A. Yetter, F.L. Dryer, A.G. Tomboulides, S.A. Orszag, Combust. Sci. Technol. 159 (2000) 199–212.
[89] C.K. Wu, C.K. Law, Proc. Combust. Inst. 20 (1984) 1941–1949.
[90] C.M. Vagelopoulos, F.N. Egolfopoulos, C.K. Law, Proc. Combust. Inst. 25 (1994) 1341–1347.
[91] D.R. Dowdy, D.B. Smith, S.C. Taylor, A. Williams, Proc. Combust. Inst. 23 (1990) 325–332.
[92] V.P. Karpov, A.N. Lipatnikov, P. Wolanski, Combust. Flame 109 (1997) 436–448.
[93] S.D. Tse, D.L. Zhu, C.K. Law, Proc. Combust. Inst. 28 (2000) 1793–1800.
[94] N. Lamoureux, N. Djebaili-Chaumeix, C.-E. Paillard, Exp. Therm. Fluid Sci. 27 (2003) 385–393.
[95] M. Ilbas, A.P. Crayford, İ. Yılmaz, P.J. Bowen, N. Syred, Int. J. Hydrogen Energy 31 (2006) 1768–1779.
[96] F.N. Egolfopoulos, C.K. Law, Proc. Combust. Inst. 23 (1990) 333–340.
[97] S. Kwon, L.-K. Tseng, G.M. Faeth, Combust. Flame 90 (1992) 230–246.
[98] X. Qin, H. Kobayashi, T. Niioka, Exp. Therm. Fluid Sci. 21 (2000) 58–63.
[99] M.J. Brown, D.B. Smith, S.C. Taylor, Combust. Flame 117 (1999) 652–656.
[100] R.T.E. Hermanns, A.A. Konnov, R.J.M. Bastiaans, L.P.H. de Goey, Energy Fuels 21 (2007) 1977–1981.
[101] G. Dixon-Lewis, M.M. Sutton, A. Williams, Proc. Combust. Inst. 10 (1965) 495–502.
[102] G. Dixon-Lewis, M.M. Sutton, A. Williams, Proc. R. Soc. London A 317 (1970) 227–234.
[103] A.A. Paletskii, L.V. Kuibida, T.A. Bolshova, O.P. Korobeinichev, R.M. Fristrom, Combust. Explos. Shock Waves 32 (3) (1996) 245–250.
[104] G. Dixon-Lewis, Philos. Trans. R. Soc. London A 292 (1979) 45–99.
[105] M. El-Gamal, E. Gutheil, J. Warnatz, Z. Phys. Chem. 214 (4) (2000) 419–435.
[106] O.E. Krivonosova, S.A. Losev, V.P. Nalivaiko, Yu.K. Mukoseev, O.P. Shatalov, in: B.M. Smirnov (Ed.), Plasma Chemistry, vol. 14, Energoatomizdat, Moscow, 1987, pp. 3–31 (in Russian).
[107] P. Glarborg, M.U. Alzueta, K. Dam-Johansen, J.A. Miller, Combust. Flame 115 (1998) 1–27.
[108] J. Peeters, G. Mahnen, Proc. Combust. Inst. 14 (1973) 133.
[109] J.M. Goodings, A.N. Hayhurst, J. Chem. Soc. Faraday Trans. 2 84 (1988) 745–762.
[110] R. Blumenthal, Doctoral thesis, Institut für Allgemeine Mechanik, RWTH Aachen, 1996, p. 44 (citation of Wang et al. [74]).
[111] D.L. Baulch, D.D. Drysdale, J. Duxbury, S.L. Grant, Evaluated Kinetic Data for High Temperature Reactions, vol. 3, Homogeneous Gas Phase Reactions of O_2–O_3 Systems, the CO–O_2–H_2 System and of Sulfur-Containing Species, Butterworths, London, 1976.
[112] L. Jerig, K. Thielen, P. Roth, AIAA J. 29 (1991) 1136–1139.
[113] V. Naudet, S. Abid, C.E. Paillard, J. Chim. Phys. 96 (1999) 1123–1145.